• U C •

FCTUC FACULDADE DE CIÊNCIAS
E TECNOLOGIA
UNIVERSIDADE DE COIMBRA

Hugo Rafael Lopes Ferreira

# Model for Angiogenesis in Three Dimensions taking into account Tissue Elasticity

*Dissertation presented to the University of Coimbra in fulfilment of the requirements necessary for obtaining a MSc degree in Physics.*

Supervisors:
Rui Travasso (CFisUC)

**Coimbra, 2016**

This project was developed in collaboration with:

*Dedicated to my parents for supporting me through all these years of study*

# *Acknowledgements*

I would like to thank my supervisor Rui Travasso for the opportunity given, to study a complex system that takes elements from both physics and biology. Also for the opportunity to get experience in the process of building a simulation of a real system.

A special thanks to Luísa for the support throughout the year and for being in the good and not so good times. And also for keeping me focussed on the work to be done even when I lost focus and for putting a smile in my lips just by being who you are.

To all my friends of "gabi", specialy Bia, Nuno, Rute e João, for the help to solve problems the arouse and the opportunity of helping them, and the times where we would just talk about other subjects that made the days that much better.

For the help in the last few critical days and the extreme availability displayed I would like to thank Pedro for the time spent trying to help me when I really needed.

Also a big thanks to the members of the group for the good environment and the eagerness to help when someone needed.

Final but definitively not least to my family and their support and understanding throughout all these years of study and helping me finish another chapter in my life.

*"The most extensive computation known has been conducted over the last billion years on a planet-wide scale: it is the evolution of life. The power of this computation is illustrated by the complexity and beauty of its crowning achievement, the human brain"*

- David Rogers

# *Abstract*

Angiogenesis is a complex problem that is present in many processes in the body, from wound healing to cancer, making it a prime target for research. In angiogenesis we have to consider several signaling pathways, from chemical signals to mechanical signals for a complete description of this process.

In this work we use a continuous model where is included the elasticity of the system, as well as the forces exerted by the endothelial cells, specially the force of the tip cell as it moves through the system following chemical signal's (vascular endothelial growth factor) gradient towards the source of the signal, the cells in hypoxia (cells with lack of oxygen). Another big part of angiogenesis is the proliferation of endothelial cells promoted by the stalk cell phenotype which is also included in the model and studied its differences with the models where no proliferation occurs. This model that includes mechanical stresses allows a better view of the influence of these stresses in angiogenesis in a three dimensional environment.

The results obtained in this work show that the model can indeed simulate, at least qualitatively, the angiogenic process and show the importance of the mechanical stresses as drivers of tip cell movement and stalk cell proliferation in the sprouting. We also study the changes effected by the inclusion of proliferation and, as expected, the proliferation allows a better growth of the sprout and to maintain the tip cell linked even in conditions where before the tip cell would disconnect from its source vessel.

# *Resumo*

A angiogénese é um mecanismo complexo que está presente em muitos processos no corpo, desde a cicatrização à angiogénese tumoral. Esta presença faz deste mecanismo um grande alvo de estudo. Na angiogénese têm de se considerar vários sinais, desde sinais químicos, como o *vascular endothelial growth factor*, a sinais mecânicos. Apenas a incorporação destas fontes de sinais permitem uma descrição completa da angiogénese.

Neste trabalho usamos um modelo contínuo onde estão incluídas as propriedades elásticas do sistema assim como as forças provocadas pelas células endoteliais, especialmente das que adquirem o fenótipo de célula ponta (*tip cell*), enquanto se movem no sistema seguindo o gradiente dos sinais químicos, que aponta na direcção das células em hipóxia (com falta de oxigénio) que são a fonte de *VEGF*. A proliferação de células endoteliais é outra parte vital da angiogénese. As células endoteliais com o fenótipo de *stalk cell* são as responsáveis pela proliferação e, neste trabalho, são estudadas as alterações na resposta do sistema quando proliferação é introduzida. A inclusão de stresses mecânicos no sistema permite estudar o efeito que estes têm sobre o processo de angiogénese num espaço tridimensional.

Os resultados obtidos neste trabalho mostram que o modelo consegue modelar, pelo menos qualitativamente, o processo de angiogénese e mostrar a importância dos stresses mecânicos como impulsionadores do movimento das célula ponta, assim como da proliferação das células endoteliais. Neste trabalho são também estudadas as alterações devido à proliferação e, como esperado, esta permite um melhor crescimento do novo vaso e consegue manter a ligação entre a célula ponta e o vaso inicial mesmo em condições onde, anteriormente, esta ligação era quebrada.

# Contents

# List of Figures

# List of Abbreviations

| | |
|---|---|
| **AJ** | **A**dheren **J**unction |
| **ECM** | **E**xtra**C**ellular **M**atrix |
| **EC** | **E**ndothelial **C**ell |
| **FA** | **F**ocal **A**dhesion |
| **QC** | **Q**uiescent **C**ell |
| **SC** | **S**talk **C**ell |
| **TC** | **T**ip **C**ell |
| **TJ** | **T**ight **J**unction |
| **VEGF** | **V**ascular **E**ndothelial **G**rowth **F**actor |

# List of Symbols

| | |
|---|---|
| $\phi$ | Order parameter |
| $\omega$ | Displacement matrix |
| $\chi$ | Applied forces |
| $\chi^f$ | Tip cell forces |
| $V$ | VEGF concentration |
| $F$ | Free energy functional |
| $\alpha$ | Adhesion constant |
| $L_0$ | Elastic constant |
| $\rho$ | Free energy density |
| $M$ | Mobility constant |
| $\mu$ | Difference of rigidity modules |
| $f$ | Force amplitude |
| $V_{max}$ | Maximum VEGF concentration |
| $P_{max}$ | Maximum proliferation |

# Chapter 1

# Introduction

## 1.1 Biological Introduction

Angiogenesis is a complex process by which new blood vessels grow from existing ones that occurs often in the human body, for example, during tissue regeneration and tumour development. There are two main types of angiogenesis: splitting (intussusception) angiogenesis where a new vessel is formed by the division of a pre-existing one into two new vessels, and sprouting angiogenesis in which new vessels are created from sprouts of the wall of pre-existing vessels (see Figure 1.1) [1]. This type of angiogenesis is the one studied in this work and so its components and agents will be detailed below.

The main topics in angiogenesis that we will discuss are cellular adhesion, i.e. how cells remain linked both to each other and to the extracellular matrix (ECM), cellular motility, describing how cells are able to move through its medium, the types of endothelial cells (EC) activation states involved along with their properties, and the communication between cells as well as how they perceive their environment.

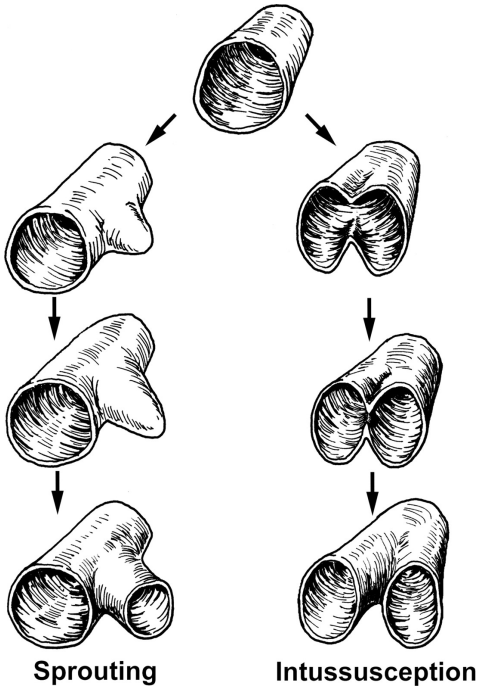


FIGURE 1.1: Evolution of the two main types of angiogenic processes (sprouting and splitting). The spouting angiogenesis is the one studied in this work. (source: Prior, Barry M., 2004 [2])

### 1.1.1 Sprouting Angiogenesis

Angiogenesis is often triggered by the accumulation of specific signalling proteins, called growth factors produced by cells in a state of hypoxia (oxygen deprivation) [3]. The most important of these is Vascular Endothelial Growth Factor (VEGF), which is the most researched and used in the study of angiogenesis. This growth factor connects to the corresponding receptor, existent in the membrane of endothelial cells of the capillary walls of a pre existing vessel, changing the genetic expression (altering its phenotype), thus jump starting the process [4].

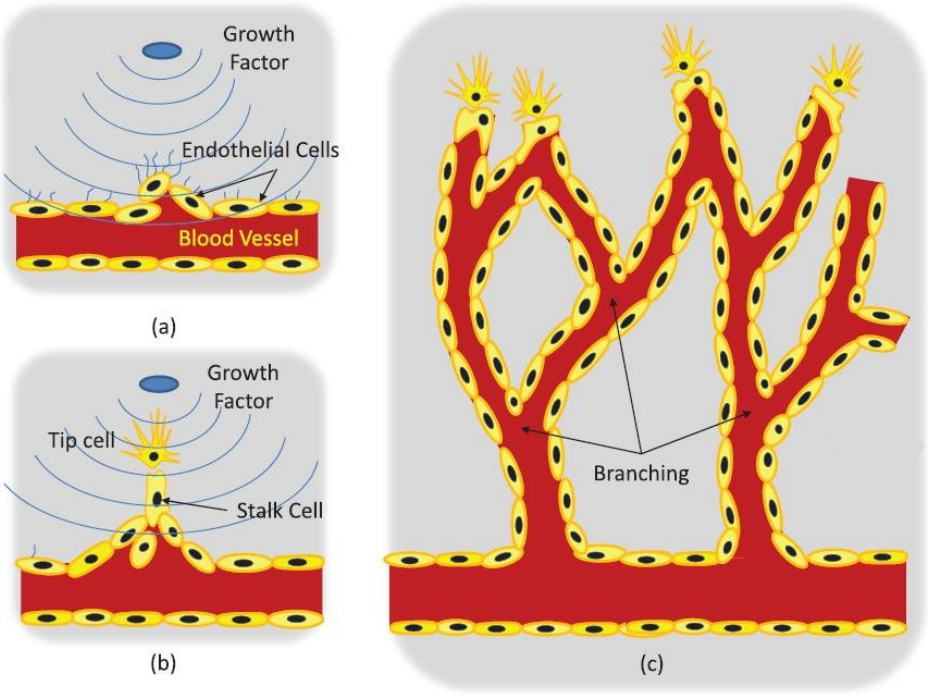


FIGURE 1.2: Depiction of the processes that trigger and sustain sprouting. We can see the distinction between Tip Cells and Stalk Cells. In the right most panel is shown a newly formed capillary network with several new branches. (source: BioSym [5])

In a normal state endothelial cells are non mobile as they are stabilized by perycites (cells that help maturing new vessels allowing them to carry blood) and a protein wall (basement membrane), this phenotype change allows ECs to produce kinases that degrade the membrane and permits the excursion of ECs into the tissue in search of the source of VEGF [6].

In sprouting angiogenesis there are three distinct types of endothelial cell states: tip (TC), stalk (SC) and phalanx or quiescent (QC) cells. The latter are cells that remain inactive and do not respond to the VEGF stimuli these are found in the capillary walls and maintain integrity of the existing vessel. Tip cells sense their environment and determine the direction that the new vessel will take while stalk cells follow them due to cell-cell adhesion. Stalk cells proliferate thus providing new cells for the growing vessel (See Figure 1.2) [1].

Tip cells have specialized filopodia that act as probes sensing their environment for the several signalling cues, be it chemical sources (chemotaxis),mechanical (mechanotaxis) or ECM rigidity sensing (durotaxis). [7] Chemotaxis is the movement of the cell due to the presence of chemical signals, the most obvious of which is VEGF, but other molecules also contribute to this signaling. [8] Mechanotaxis is movement triggered by signals produced due to the presence of a mechanical force, like shear stress from blood flow and durotaxis is a movement closely tied to the rigidity of the local ECM. The combination of these signals give information to the cell chose the path to follow [9].

It is obvious that not all endothelial cells can be Tip cells as that would destroy the existing vessel. There is a mechanism that stops ECs from becoming a Tip cell if there is already one nearby (i.e if it is neighbour to a tip cell), this mechanism uses the Notch signalling pathway with the Delta-like ligand 4 (Dll4) which down regulates the tip cell phenotype by lowering the levels of VEGF receptors in Notch activated cells, stopping them from becoming Tip cells. The Notch activated cells become the stalk cells [10].

This system opens a question of how the Tip cells are chosen as, in the beginning, most cells are in, roughly, the same conditions. Recent studies have shown indeed that the cell designated TC is not static but there is a competition between the endothelial cells at the front of the growing sprout [11]. The EC that as the stronger signal becomes a Tip cell and the others around become Stalk cells. Another factor that influences this competition is, in fact, that different cells can have varying amounts of VEGF receptors leading to differing sensitiveness to the signal [1].

Stalk cells are then pulled along by the migrating TCs, due to the cell-to-cell adhesion junctions detailed in the next section. These cells will proliferate, allowing the sprout to remain connected to the starting vessel. VEGF and other growth factors as well as the mechanical stimulus, due to traction forces, control the proliferation rates of the stalk cells [9].

When two of these new sprouts meet, they form a loop which begins maturing, promoting the migration and proliferation of perycites, that return the endothelial cells to a quiescent state. The basement membrane starts forming, a lumen is formed, and the new vessel is capable of sustaining blood flow, relieving the hypoxia in the area, and leading to a final maturing process until the vessel is fully formed and the angiogenesis stops [12].

### 1.1.2 Cell Adhesion

In cell adhesion participate hundreds of different proteins and reaction chains. In this section we shall discuss the most relevant agents involved in cell-to-cell and cell-to-Extracellular Matrix adhesion processes for the mechanisms involved in angiogenesis (Figure 1.3). [13]

#### Cell-to-Cell Adhesion

Endothelial cells neighbouring each other have adhesion points between them, these are given the name of junctions. There are mainly three types of these junctions with distinct functions: gap, adherens (AJ) and tight (TJ) junctions [15].

The gap junction's main function is intercellular communication through the transport of small molecular weight molecules and ions, these junctions may provide a mechanism for endothelial cell coordination during angiogenesis. Tight junctions regulate the paracellular permeability (regulating the transport across intercellular space between cells) as well as maintaining cell polarity (related to shape of the cell). The AJs allow cells to adhere to each other and to create strong binding zones [16]. While all junctions play a part in the processes involving endothelial cells, we shall have a closer look at AJs as these are more relevant for our study of mechanical forces in endothelial cells.

Adherens junctions are formed by complex protein complexes, the principal component being proteins from the cadherin family, several distinct types have indeed been found in the membrane of endothelial cells. In contrast with other cellular types, ECs have a special protein of this family, the vascular endothelial cadherin (VE-cadherin), along with the normal N-cadherin and others [15]. More than being the building block for endothelial cell AJs, VE-cadherins are also necessary for EC survival, indeed it was shown that lack of expression of VE-cadherins leads to cell apoptosis [17].

The N-cadherins are, normally, the base for AJs however, in endothelial cells, these are spread across the cellular membrane while the VE-cadherins take responsibility for the formation of these junctions [18]. VE-cadherins have three parts: one outside the cell that connects to other cadherin, the transmembrane part and an internal part, the last one connecting

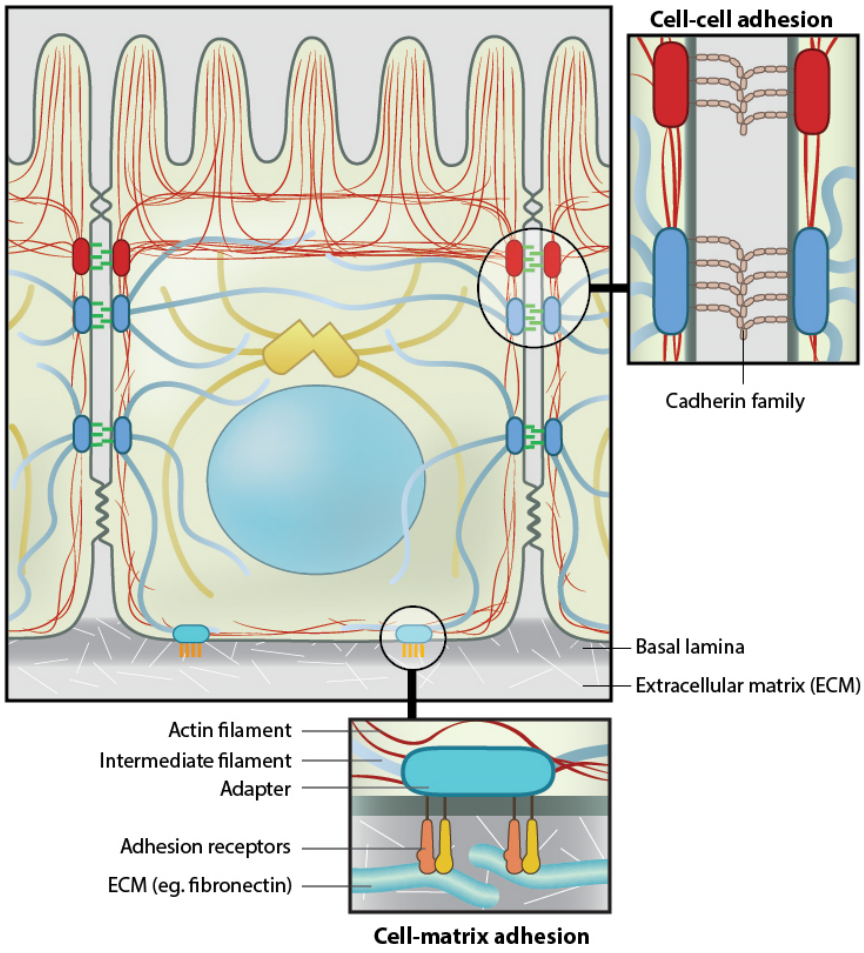


FIGURE 1.3: Schematic representation of cell-to-cell and cell-to-ECM adhesions. In the zoomed regions are detailed views of these connections and their principal components. Actin filaments are shown in red, the microtubules in yellow and the intermediate filaments in blue. Oval shapes represent transmembrane complexes. (source: MB:Info [14])

to proteins called catenins, which in turn connect to actin fibres of the cytoskeleton. This junction allows then the connection of the cytoskeletons of the two cells that participate in the AJ, thus creating a strong bond between them [16].

These special AJ formed by VE-cadherin have some additional properties which are of interest, like binding to the VEGF receptor 2 (VEGFR2). When this structure is activated it mediates the phosphorilation of VE-cadherin creating a signal inside the cell. Indeed the truncation of the intracellular part of the VE-cadherins impaired the VEGF signalling, inducing endothelial apoptosis. This process also weakens the junction and, as an antagonist for this phosphorilation, VE-cadherins can interact with a protein receptor tyrosine phosphatase (VE-PTP) that reduces the reaction and maintains the adhesion strength of AJ [16]. The activation of this complex can occur by VEGF activation or by mechanosensing through the shear stress produced by blood flow [19].

### Cell-to-Extracellular Matrix Adhesion

The extracellular matrix (ECM) is a collection of molecules that provides structural and biochemical support to the neighbouring cells [20]. The major components are fibers that make the bulk of the ECM such as collagen, that makes the majority of the ECM, elastin that confers elasticity to the ECM and fibronectin. Studies have revealed another important contribution

of the ECM to endothelial cells, as a survival factor for these. Indeed cells where the ability to form focal adhesions with the ECM was impeded would rapidly enter apoptosis [21].

The integrins are transmembrane receptors that functions as adhesion molecules, participating in cell-cell and cell-ECM connections. These receptors however have the spotlight in cell-ECM adhesion connecting to all major fibers existing in the ECM allowing support of the cell [22]. These connections are focal adhesions (FAs). Focal adhesions are complex structures formed from integrins and some other 100 different proteins and, as a parallel with Adherens junctions, they do more than just anchor the cell, they serve also as sensors detailing the state of the surrounding ECM. FAs are, under normal circumstances, quite stable. This stability is reduced however in moving cells where the FAs are on a constant state of assembling (leading edge) and disassembling (trailing edge) allowing the cell to effectively move [13].

### 1.1.3 Cell Motility

Here we offer a brief overview of the movement of endothelial cells during migration. ECs can move due to several signal types, be it a chemical signal like the gradient of VEGF or other signalling molecules (chemotaxis) or information on the gradient of adhesion sites (haptotaxis) or even the perception of the rigidity gradient of the ECM in their surroundings (durotaxis). These three different signals work in tandem to give complete information to the cell not only of where to go but also what path is the easiest to reach the desired destination (tissue in hypoxia and source of VEGF) [6].

Cell motility is very dependent of cell-ECM adhesion as the focal adhesions provide anchor locations and allow the cell to pull itself forward and to attach to a new adhesion site [23]. The strength of the focal adhesions is however a double edged sword for the cell, as the higher stability means increased force but also leads to difficulty in detaching from the ECM at the trailing edge of the cell. The opposite problem can occur too if the cell is only weakly linked to the ECM as it will only be able to produce small amounts of force reducing its movement speed. In this context different types of cells take different approaches to deal with this situation. [6]. In this work we wont go to specifics about the molecular mechanisms of adhesion. We will assume that the cells are capable of doing a specific amount of force that we can control, and changing it will let us study several different cases of varying cell-ECM adhesion strength.

## 1.2 Models Overview

Computational models are expanding their presence in modelling biological systems allowing, along with experimentation, a faster and better search for models that represent the reality. These models can serve a variety of roles, from theory testing to suggesting alternative hypothesis or integrating knowledge. For their versatility they are increasingly important in the exploration of the frontiers of our understanding of the subject in study [24].

Angiogenesis is an important topic in many biological processes, and as such it is widely studied in a variety of levels: from the most basic reaction networks to cell population level, each level concerning itself with parts of this system [25].

There are several approaches to study this problem, cell based modelling [26], where each cell is simulated and cell population models [27], where we abstract from the individual cells and threat them as part of a population.

Cell based modelling can be useful if one wants to study the formation of macrostructures, such as new vessels, from their individual components and the interactions between all the cells involved in the process. These models also allow the study of changes in cells necessary for the processes in study to occur. The main drawbacks of these types of models are the large number of parameters required, and the large amount of cells needed to simulate even small parts of the angiogenic process, which leads to large computational time.

Cell Population models use an abstract variable that defines the cells and their position using diffusion equations to model their movement and interaction dynamics. With this abstraction we can lower the computational cost of modelling the system, however this comes at the cost of losing accuracy in the results but also lowers the number of parameters needed for the model.

In this work we use cell population and tissue characteristics instead of single cell models or reaction network models, as our aim is to study the influence of mechanical properties and responses of the cells in the process of angiogenesis, and how these affect the morphology of the newly formed vessel.

## 1.3 Objectives and Motivation

The vascular system is fundamental for complex organisms, making possible the distribution of oxygen and nutrients to all cells as well as carrying away metabolic byproducts that would otherwise poison the cells that produce them [28]. For this system to be competent at its function is imperative the maintenance of existing vessels as well as the *de novo* formation of vessels. Angiogenesis (blood vessel growth) is then an important mechanism in our body.

Naturally, such far reaching process influences many aspects of the normal or disease-related functions such as tissue regeneration, tumour development and other diseases [28]. The study and further comprehension of such mechanism is essential to the understanding of the workings of many processes that take place in our body, as well as contributing to a more informed view of some diseases, possibly opening new avenues of control or treatment.

The exploit of this mechanism was first used as part of cancer treatment, by reducing angiogenesis near the tumour cells it was hoped that these would die through hypoxia, and indeed some would die, though long term benefits could not be achieved [13]. Now we know that this treatment would promote selective pressure on tumour cells, leaving the more aggressive, and motile, alive leading to faster metastasization of the tumour in remote organs [4]. Knowing this, instead of focusing in killing the tumour by starvation, researchers turned to normalizing the vasculature created by tumours for more effective delivery of chemotherapy drugs and radiation therapy [12], and to decrease the size of hypoxic regions in the tumour site. Normalization of the vasculature demands, however, specific amounts of anti-angiogenic agents only possible by in-depth knowledge of the complex web of interactions during angiogenesis, both biological and mechanical.

Angiogenesis is a strongly three dimensional phenomenon: the description of the shape of the vessel and of the manner the cells rearrange in space and move, require three dimensions. However all continuous models of angiogenesis in the literature that take into account the mechanical effects are written in two dimensions. In the present work, we will open the grounds for the development of a three dimensional model of angiogenesis that takes into account the tissue's elasticity. The aim of this work is therefore to create the basis for this model, and not to obtain a final description of vessel growth in 3D. For this reason, we will present our results in arbitrary units and observe the plausibility of the vessel formations observed.

# Chapter 2

# Model Development

## 2.1 Origin and base model

The model used in this work is a phase field model, initially developed for non-equilibrium physics in the study of phase separation in metals. The central point of these models is a field ($\phi$), and the dynamics of the system in study is then derived for this field. In this chapter we will detail the process to obtain such equations for the dynamics of the phase field in order to represent sprouting angiogenesis.

The starting point is the Allen-Cahn equation, a deterministic version of the dynamics of an Ising model, which has the form:

$$\frac{\partial \phi(\mathbf{r},t)}{\partial t} = -D\frac{\delta F[\phi(\mathbf{r},t)]}{\delta \phi(\mathbf{r},t)}. \tag{2.1}$$

Where $D$ is the diffusion constant of our problem and $F$ is the free energy functional suitable for the particular system in study.

In this work we need a tight control over the conservation of the field, the non conservation will be equated to the proliferation of cells, and the equation above does not meet that demand. To that end and using the previous equation as a base, we can obtain a similar equation that respects phase conservation.

We start from a continuity equation:

$$\frac{\partial \phi}{\partial t} + \nabla \cdot \mathbf{j} = 0. \tag{2.2}$$

Setting the phase flux $\mathbf{j}$ as $-D\nabla\frac{\delta F}{\delta \phi}$, the continuity equation becomes:

$$\frac{\partial \phi(\mathbf{r},t)}{\partial t} = D\nabla^2\left(\frac{\delta F[\phi(\mathbf{r},t)]}{\delta \phi(\mathbf{r},t)}\right). \tag{2.3}$$

This is the equation that we work with, the specific description of the system is contained in the free energy functional. We use the Ginzburg-Landau functional with the form:

$$F[\phi(\mathbf{r},t)] = \int \Big[f(\phi(\mathbf{r},t)) + \frac{\epsilon^2}{2}(\nabla\phi(\mathbf{r},t))^2\Big]d\mathbf{r}. \tag{2.4}$$

Where f is the local free energy functional and $\epsilon$ is the interface width between phases. This local free energy will, for now, take form as to give an energy minima for two values of the phase, considered $+1$ and $-1$ (see Figure 2.1). In this way, $F[\phi(\mathbf{r},t)]$ ir written as a double well potential:

$$f[\phi(\mathbf{r},t)] = \frac{\phi(\mathbf{r},t)^4}{4} - \frac{\phi(\mathbf{r},t)^2}{2}. \tag{2.5}$$

Using the equations above and computing the functional derivative with respect to $\phi$ (detailed in Appendix A) we get the Cahn-Hilliard equation:

$$\frac{\partial \phi(\mathbf{r},t)}{\partial t} = D\nabla^2\Big(-\phi(\mathbf{r},t) + \phi(\mathbf{r},t)^3 - \epsilon^2\nabla^2\phi(\mathbf{r},t)\Big). \tag{2.6}$$

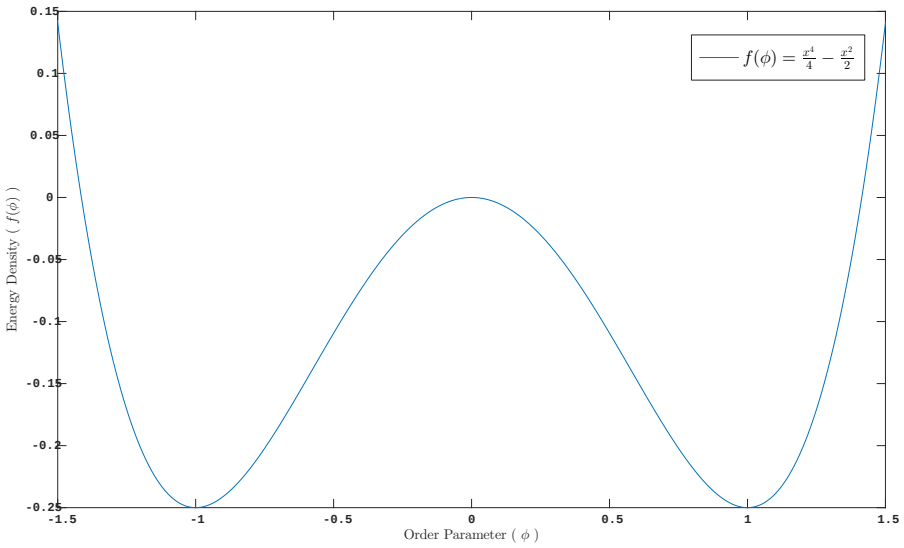


FIGURE 2.1: Energy density function, giving two minima for $\phi$ values of +1 and -1.

## 2.2 Including Mechanical Properties

Having the framework for the time evolution of the phase field and a base free energy that allows the existence of two separate phases (that we consider as the vessel and the extracellular matrix), now the next step is to include the mechanical properties of the system in the free energy functional, including the elastic energy associated with phase displacement and the energy contribution of the forces created by the cells (more specifically the tip cells).

The elastic energy has the initial form:

$$F_{ele}[\mathbf{u}(\mathbf{r})] = \int \frac{1}{2}(\sigma : \varepsilon) d\mathbf{r}. \tag{2.7}$$

Where $\varepsilon$ is the strain tensor whose elements are given by:

$$\varepsilon_{ij} = \frac{1}{2}(\partial_i u_j + \partial_j u_i). \tag{2.8}$$

The stress tensor ($\sigma$) here used for the model derivation assumes that the system is homogeneous and isotropic. In this constraints the elements of this tensor have the following form:

$$\sigma_{ij} = K\delta_{ij}\varepsilon_{kk} + 2\mu\left(\varepsilon_{ij} - \frac{\delta_{ij}}{d}\varepsilon_{kk}\right). \tag{2.9}$$

Where $K$ is the compressibility modulus, $\mu$ the rigidity modulus, $d$ the dimensionality of the system in study and $\delta_{ij}$ is the Kronecker delta.

The cell forces contribution to the free energy functional:

$$F_f[\phi(\mathbf{r}), \mathbf{u}(\mathbf{r})] = -\int \chi \nabla \cdot \mathbf{u}(\mathbf{r}) d\mathbf{r}. \tag{2.10}$$

The field $\mathbf{u}(\mathbf{r})$ is the displacement field and $\chi$ is defined as a field whose gradient is proportional to the applied forces in the system. Here were considered two sources, the adhesion force that tries to maintain the dominions together, mimicking the cell-cell attraction mediated by the adhesion molecules discussed in 1. This force's direction is towards increasing

values of $\phi$ and effectively acts as a balance to the other force. The second source is the pulling created by the TC as it tries to move, in this work we will assume that this force is completely independent from the order parameter. It is also assumed the tip cell to be spherical giving the force a cylindrical symmetry whose long axis is the direction of the force.

The field $\chi$ can then be written as a sum of potentials of these two forces (where $\chi^f$ denotes the contribution of the TC force):

$$\chi = -\alpha\phi + \chi^f. \tag{2.11}$$

### 2.2.1 Derivation of the mechanical contribution

In this system we consider the relaxation of the displacement field to be much faster than the order parameter's and, as such, we can treat the system as being in a state of mechanical equilibrium leading to the equation:

$$\frac{\delta F}{\delta u_i} = 0 = \frac{\delta F_{ele}}{\delta u_i} + \frac{\delta F_f}{\delta u_i}. \tag{2.12}$$

In order to continue the study of the mechanical part of the system we need to do some approximations. First we shall consider a small difference between the rigidity moduli of the two phases ($\mu = \mu_0 - \phi\mu_1$), where $\mu_1 \ll \mu_0$. We can also split the displacement field $\mathbf{u} = \mathbf{u}^0 + \mathbf{u}^1$ and the energy functional. The specific calculations for the results bellow are detailed in Appendix B. When using $f$ in this work it is referring to the equation inside the integral (e.g. $f_{ele} = \frac{1}{2}\sigma : \varepsilon$)

Calculating the functional derivative of the elastic energy term with respect to the displacement field, maintaining the order zero terms and considering a new field $\omega$ such that $\nabla\omega = \mathbf{u^0}(\mathbf{r})$, yields:

$$\frac{\delta F_{ele}}{\delta u_i^0} = -\left(K - \frac{2\mu_0}{d}\right)\partial_{ij}u_j^0 - \mu_0(\partial_{ij}u_j^0 + \partial_{jj}u_i^0) = -\left(K - \frac{2\mu_0}{d} + 2\mu_0\right)\partial_{ijj}\omega = -L_0\partial_{ijj}\omega. \tag{2.13}$$

Where $L_0$ condenses the constants for easier manipulation of the equations. Knowing that the total derivative with respect to displacement field must be zero and where $\frac{\delta F_f}{\delta u_i} = -\partial_i\chi$, it follows that $-L_0\partial_{ijj}\omega + \partial_i\chi = 0$, which is satisfied by:

$$L_0\nabla^2\omega = \chi = -\alpha\phi + \chi^f. \tag{2.14}$$

Rewriting the zero order of the energy functional in terms of $\omega$ yields (Appendix C):

$$F_{mec}^0 = -\int \frac{1}{2}(\chi\nabla^2\omega)d\mathbf{r} = -\int \frac{\chi^2}{2L_0}d\mathbf{r}. \tag{2.15}$$

With this result we have another term of the energy functional ready, the final term comes from the same process this time gathering the first order terms of the mechanical energy functional. Again as detailed in Appendix B, we notice that the terms containing $\mathbf{u^1}(\mathbf{r})$ cancel out leaving only the terms proportional to $\mu_1$:

$$F_{mec}^1 = -\int \mu_1\phi\left(\partial_{ij}\omega\partial_{ij}\omega - \frac{1}{d}(\nabla^2\omega)^2\right)d\mathbf{r}. \tag{2.16}$$

## 2.3 Final equations

The full equation for the free energy functional of the system is:

$$F[\phi(\mathbf{r}),\mathbf{u}(\mathbf{r})]=\int\left[\rho_\phi\left(-\frac{a\phi^2}{2}+\frac{\phi^4}{4}+\frac{\epsilon^2}{2}(\nabla^2\phi)^2\right)-\frac{\chi^2}{2L_0}-\mu_1\phi\left(\partial_{ij}\omega\partial_{ij}\omega-\frac{1}{d}(\nabla^2\omega)^2\right)\right]d\mathbf{r}. \tag{2.17}$$

Using all of the tools above we can compute the derivative with respect to the order parameter (Appendix D). Plugging the resulting equation to the time derivative equation for the order parameter ($\frac{\partial\phi}{\partial t}=M\nabla^2\frac{\delta F}{\delta\phi}$), yields:

$$\frac{1}{M}\frac{\partial\phi}{\partial t}=\nabla^2\left(\rho_\phi(-\phi+\phi^3-\epsilon^2\nabla^2\phi)+\frac{\alpha\chi^f}{L_0}\right)-\mu_1\nabla^2\left(\partial_{ij}w\partial_{ij}w-\frac{1}{d}(\nabla^2w)^2\right)+\frac{2\mu_1\alpha}{L_0}\partial_{ij}\left[\phi\left(\partial_{ij}w-\frac{\delta_{ij}}{d}\nabla^2w\right)\right]. \tag{2.18}$$

This equation is solved together with the equation to determine the auxiliary field $\omega$:

$$L_0\nabla^2w=-\alpha\phi+\chi^f. \tag{2.19}$$

## 2.4 Tip cell force

To simplify the calculation of the $\chi^f$ field we shall confine the force created by the tip cell allowing us to have a local solution to both the field and the force. To compute $\chi^f$ the following equation is used:

$$\nabla^2\chi^f=-\nabla\cdot\mathbf{f^{tc}}. \tag{2.20}$$

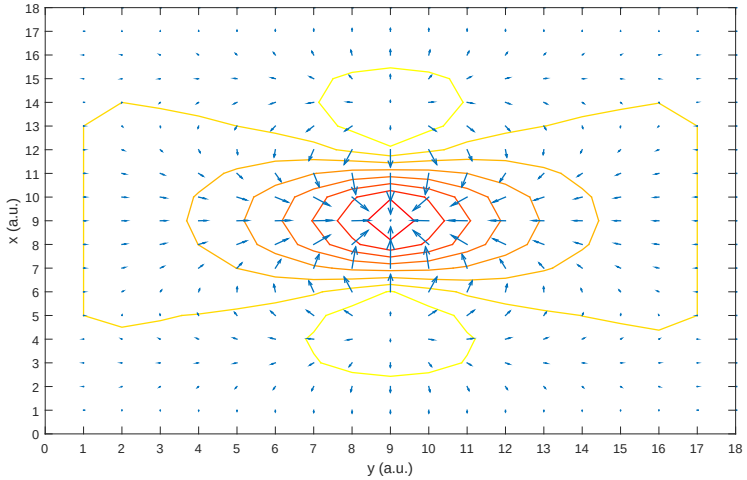


FIGURE 2.2: A slice of the force field of a tip cell (z-constant plane). The contour lines are the isolines of $\chi$ field. This force is the force profile used in this work and is calculated indirectly through equation 2.20.

Solving it with the boundary condition set as $\chi^f=0$, we indeed get a local solution. In this equation, $\mathbf{f^{tc}}$ is only a prototype for the force. Having solved this equation we can then reverse it, obtaining the "real" force, that automatically complies with the boundary condition set above. This is the actual force that is used in the system, as displayed in the figure 2.2.

This same setup can be used for more complex force distributions like the fields measured experimentally (Figure 2.3) by setting $f^{tc}$ with that data. Here a dipole like force field was used as the base for the tip cell force.

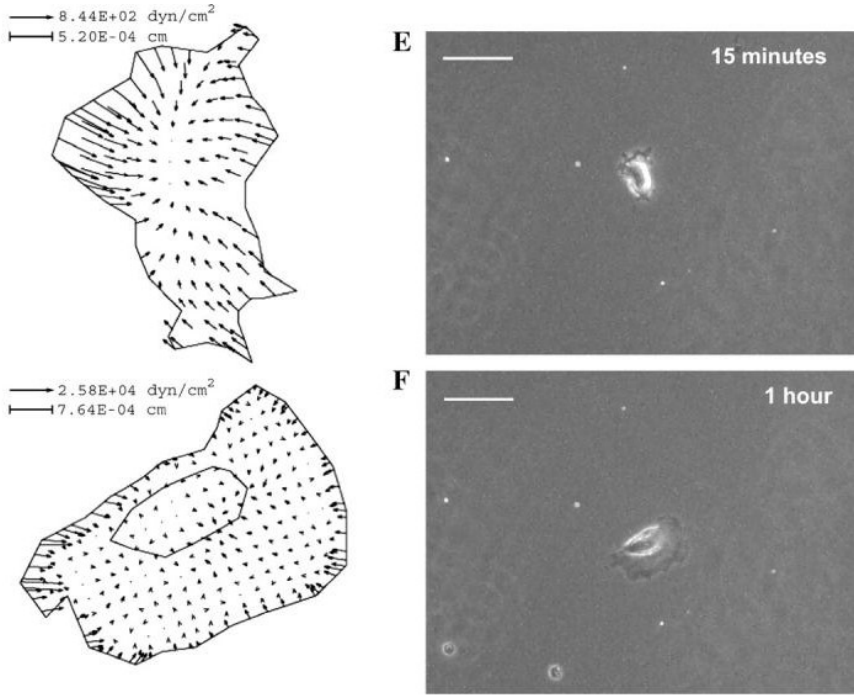


FIGURE 2.3: Results of force microscopy performed on an endothelial cell. It can be seen similarities with the chosen force in this work. Both have a force that pushes to the center of the cell from its periphery. (source: [29])

## 2.5 VEGF dynamics

As discussed in Chapter 1, one main driving factor of angiogenesis is VEFG signaling. In this work we simulate a VEGF system where we have a source of the signal which diffuses to its surroundings. Endothelial cells in contact with a VEGF concentration will consume part of this concentration due to the binding with the appropriate receptors. This dynamic of VEGF is modelled by the following diffusion equation:

$$\frac{\partial V}{\partial t} = D_v \nabla^2 V - \alpha_v V \phi \Theta(\phi), \tag{2.21}$$

Where $D_v$ is the diffusion constant, $\alpha_v$ is the consumption rate by the endothelial cells and $\Theta(\phi)$ is the Heaviside function which allows consumption only where $\phi$ that corresponds to the presence of endothelial cells. The penetration width of VEGF into endothelial tissue is given by the constant ratio $\sqrt{D_v/\alpha_v}$.

## 2.6 Proliferation

The proliferation, in this model, is a local value that is the average proliferation in a volume the size of a cell. The equation for this being:

$$\alpha_p(V, \phi, \omega) = \frac{\int_\Omega p(V, \omega)\Theta(\phi) d\mathbf{r}}{\int_\Omega \Theta(\phi) d\mathbf{r}}, \tag{2.22}$$

Where $\Omega$ is the cell volume, $\Theta(\phi)$ is the Heaviside function and $p(V, \omega)$ is the proliferation function used for this model, and we consider that both VEGF concentration and strain contribute to proliferation.

For the strain dependence it is assumed that a minimum strain must be present in order to exist proliferation, and so a Heaviside function is used ($\Theta(\nabla^2\omega + \alpha - T_{limit})$), where $T_{limit}$ is that imposed minimum strain on proliferation.

The dependence on V is characterised by two sections, a linear and a saturated part. When the VEGF value is smaller than a maximum ($V_{max}$) then the proliferation grows linearly with V. Above that value though the proliferation saturates ($P_{max}$), this mimics the limited rate of proliferation of endothelial cells. The proliferation dependence on V yields:

$$p(V) = \begin{cases} \frac{P_{max}}{V_{max}} V, & V < V_{max} \\ P_{max}, & V > V_{max} \end{cases}. \tag{2.23}$$

The total $p$ function gives:

$$p(V, \omega) = \Theta(\nabla^2 \omega + \alpha - T_{limit}) \begin{cases} \frac{P_{max}}{V_{max}} V, & V < V_{max} \\ P_{max}, & V > V_{max} \end{cases}. \tag{2.24}$$

# Chapter 3

# Computational Implementation

Having a mathematical model for the system, the following step is its conversion to a computational model that can be coded and run on a computer. The base for the simulation of this system stands on the discretization of the spacial coordinates, meaning that, in computational terms, each field will be a three dimensional matrix. The values of the fields in each point of the lattice space will still be a continuous variable.

The simulation used periodic boundary conditions for most of the equations simulated unless it is specified in each section of this chapter.

## 3.1 Order parameter

The order parameter uses the equation found in Chapter 2 leading to the equation:

$$\frac{\partial\phi(t,\mathbf{r})}{\partial t} \simeq \frac{\phi(t+\Delta t,\mathbf{r})-\phi(t,\mathbf{r})}{\Delta t} \Leftrightarrow \phi(t+\Delta t,\mathbf{r}) = \phi(t) + \Delta t\frac{\partial\phi(t,\mathbf{r})}{\partial t} \tag{3.1}$$

Where the derivatives found in $\frac{\partial\phi}{\partial t}$ are computed using the finite differences method. This method uses the derivative definition to get an approximate value for the derivative in question (here used first order approximation only). Bellow are detailed the different derivatives used and their expressions using this method.

$$\frac{\partial f(x,y,z)}{\partial x} \simeq \frac{f(x+h,y,z)-f(x-h,y,z)}{2h} \tag{3.2}$$

$$\frac{\partial^2 f(x,y,z)}{\partial x^2} \simeq \frac{f(x+h,y,z)+f(x-h,y,z)-2f(x,y,z)}{h^2} \tag{3.3}$$

$$\frac{\partial^2 f(x,y,z)}{\partial x\partial y} \simeq \frac{f(x+h,y+h,z)+f(x-h,y-h,z)-f(x+h,y-h,z)-f(x-h,y+h,z)}{4h^2} \tag{3.4}$$

$$\begin{aligned}\nabla^2 f(x,y,z) \simeq \frac{1}{h^2}\big[&f(x+h,y,z)+f(x-h,y,z)+f(x,y+h,z)+f(x,y-h,z)+\\&+f(x,y,z+h)+f(x,y,z+h)-6f(x,y,z)\big]\end{aligned} \tag{3.5}$$

The full equation for the time evolution of the order parameter is rather long and complex and, instead of computing it in one line, it was sectioned so that parts of the equation could be computed first and then put together in the final calculation, this allows a clearer view of the calculations done and easier debug of this part of the program (see Figure 3.1).

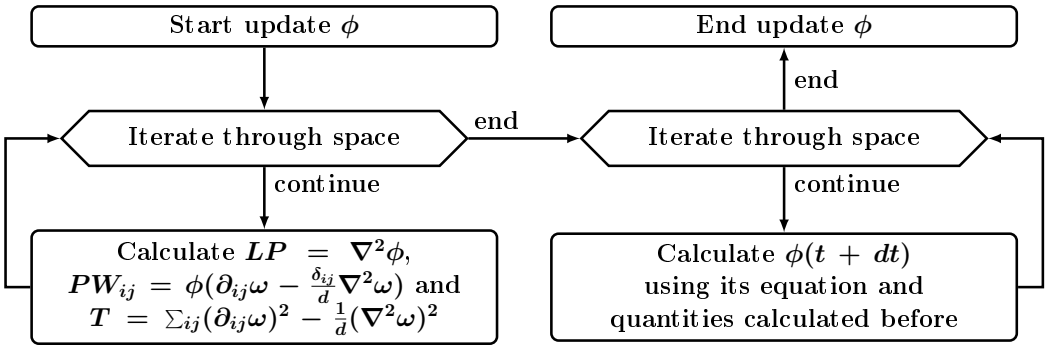


FIGURE 3.1: Fluxogram detailing the process used to update the order parameter at each time step. As discussed above the calculation is divided in two stages where some quantities are calculated before the final calculation to update $\phi$.

## 3.2 Evolution of $\omega$

As detailed in the previous Chapter we considered the system in mechanical equilibrium. This leads to the field $\omega$ not having an explicit time evolution equation. Instead we have a spacial equation which we solve using the Jacobi method. This iterative method allows the calculation of the field $\omega$ at each time step until convergence is achieved. The boundary condition for this field was chosen so that its mean value is zero. This special condition is the reason that the Jacobi method is used and not other similar methods which are faster, because those don't easily deal with that type of boundary conditions. The equation used for this calculation (also using finite differences) is the following:

$$\begin{aligned}\nabla^2\omega = -\alpha\phi + \chi^f \Leftrightarrow \\ \omega^{n+1}(x,y,z) = \omega^n(x+1,y,z) + \omega^n(x-1,y,z) + \omega^n(x,y+1,z) + \omega^n(x,y-1,z) + \\ \omega^n(x,y,z+1) + \omega^n(x,y,z-1) - 6\omega^n(x,y,z) + \frac{h^2}{L_0}\Big(\alpha\phi(x,y,z) - \chi^f(x,y,z)\Big)\end{aligned} \quad (3.6)$$

The fluxogram in Figure 3.2 illustrates the algorithm that calculates the $\omega$ field:

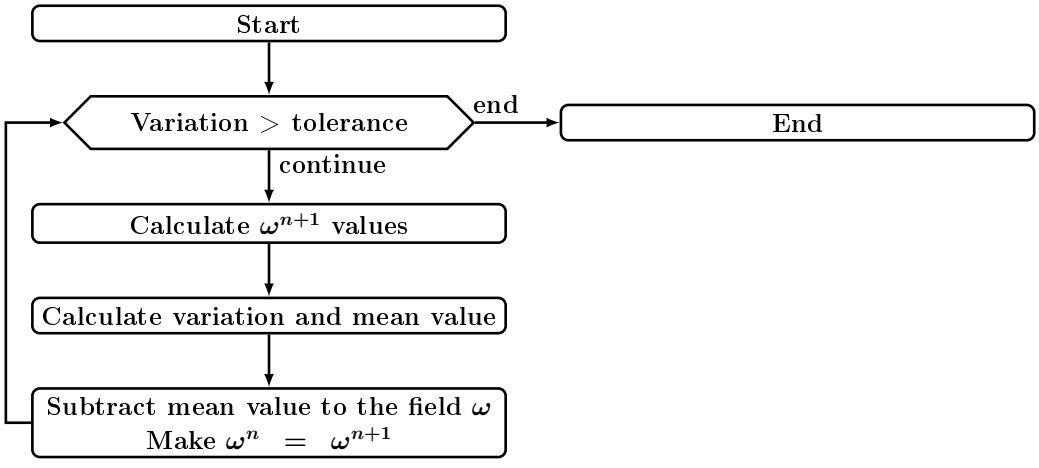


FIGURE 3.2: Fluxogram that visualizes the algorithm used for the determination of the $\omega$ field values at each time step of the program.

## 3.3 VEGF simulation

The simulation of the VEGF dynamics are quite simple as it involves diffusion of VEGF and its consumption in the vessel area. This allows the model to give cues as to the direction of tip cell movement and the consumption emulates the VEGF binding to the receptor in the cell membrane of the endothelial cells that make the vessel. The simulation then uses the same principles as the time evolution of $\phi$:

$$V(t+\Delta t, x, y, z) = V(t, x, y, z) + \frac{\partial V(t, x, y, z)}{\partial t} \cdot \Delta t = V(t, x, y, z) + \Big( D_v \nabla^2 V(t, x, y, z) - \alpha_v \Theta(\phi) \Big) \Delta t \tag{3.7}$$

Where, again, the laplacian operator is substituted by the corresponding finite differences equation described in section 3.1.

## 3.4 Tip cell movement

The movement of the tip cells in the system is much slower than the time step required for the other systems present in the model. As such, the update regarding the position of the tip cell and, as a consequence, where its force is applied, are done in bigger interval steps. This also allows for a faster simulation as the process to trace the position of TC can be calculation heavy.

The tip cell position is defined as a point in space in the frontier of the interface (where the target $\phi$ value was zero) and its direction of movement is calculated from a weighted average of the VEGF concentration gradient in a defined area, considered to be the tip cell space and the immediate neighbourhood.

When an update occurs, this direction is recalculated and, based on that result, a new position is calculated starting from a few steps behind the current tip cell position until it reaches a position that closely corresponds to $\phi = 0$. Those coordinates are then taken as the updated position of the TC and then calculates the force starting of that position.

The fluxogram of Figure 3.3 illustrates the process of update of the tip cell as described above.

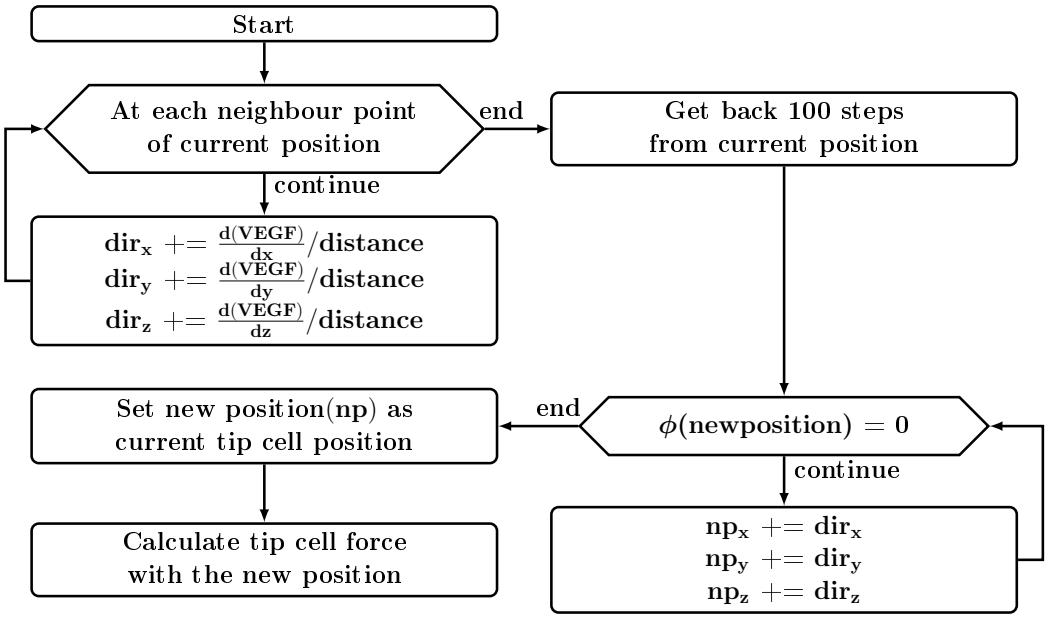


FIGURE 3.3: In this fluxogram is shown the process by which a new position is chosen for the tip cell and the update to the force generated by it.

## 3.5 $\chi^f$ update

The update of the $\chi^f$ field is done once the tip cell position is updated. This update of the tip cell gives a direction of movement which is used to calculate the force for the tip cell in the new position. Having the force we can then calculate the corresponding $\chi^f$ field using the equation in Chapter 2. In terms of computation a trick was used, instead of rotating the force, the divergence is rotated allowing the use of a single rotation to get the same effect. This algorithm is shown in Figure 3.4.

The specific equation that gives the updated values of this field:

$$\begin{aligned}\nabla^2\chi^f = -\nabla\cdot f \Leftrightarrow \\ \Leftrightarrow \chi^f_{n+1} = \Bigg(\chi^f_n(x+1,y,z)+\chi^f_n(x-1,y,z)+\chi^f_n(x,y+1,z)+\chi^f_n(x,y-1,z)+ \\ \chi^f_n(x,y,z+1)+\chi^f_n(x,y,z-1)+h^2 div_f(x,y,z)\Bigg)\frac{w}{6}+(1-w)\chi^f(x,y,z) \quad (3.8)\end{aligned}$$

Where we used again the finite differences method for the derivatives and used the over relaxation method (which $w$ is a parameter of) for the convergence of the values of the field as done with the $\omega$ field.

## 3.6 Including proliferation

The inclusion of proliferation is done in a similar way as the VEGF consumption, in that proliferation can only occur in the vessel, and under favourable conditions such as being near the interface between vessel and ECM or being in a area suffering distension. This proliferation occurs in the stalk endothelial cell state, that are near the tip cell, and their main job, as discussed in Chapter 1, is the proliferation as a source of cells for the growing sprout and maintaining the sprouts connection to the source vessel.

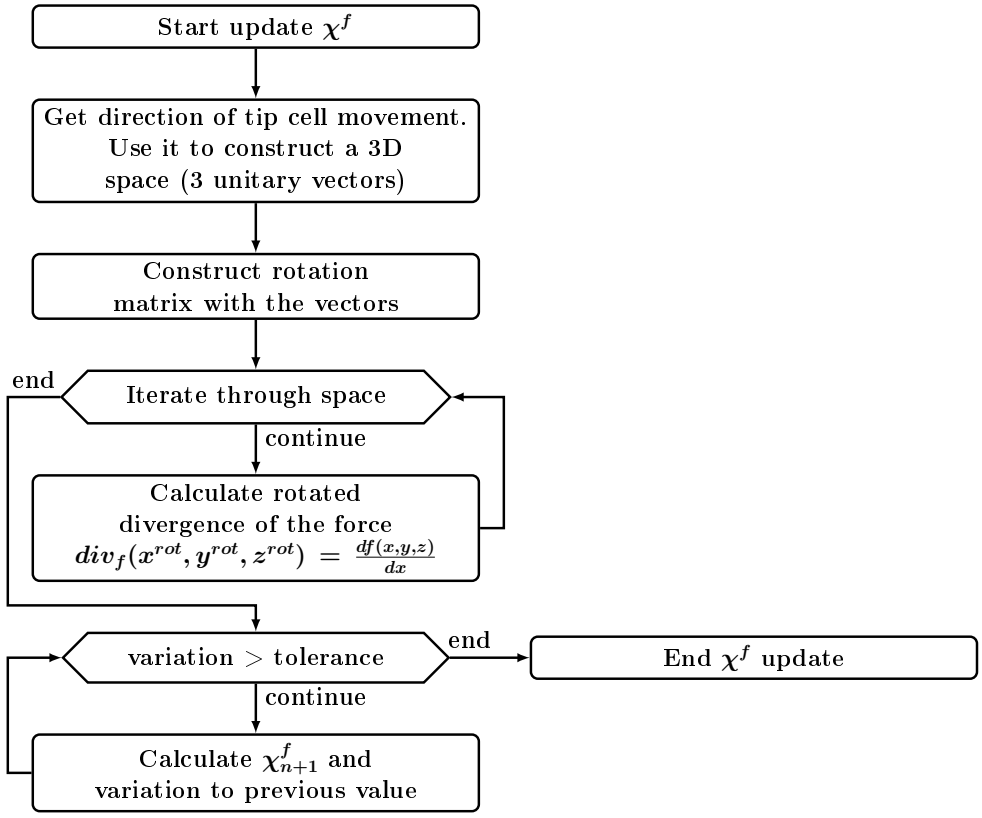


FIGURE 3.4: Schematic representation of the rotation and $\chi^f$ value determination algorithms used in this work. The rotation is done using the direction of movement of the tip cell and using some assumptions which can be done because the chosen force has cylindrical symmetry whose axis is the direction of movement. The determination of $\chi^f$ uses the over relaxation method which can be used here leading to a fast convergence for the values of the field.

The calculated term is then added to the time evolution equation for $\phi$:

$$\frac{\partial \phi(t, \mathbf{r})}{\partial t} \simeq \phi(t) + \Delta t \frac{\partial \phi(t, \mathbf{r})}{\partial t} + \Delta t \alpha_p(\phi, V, \chi^f). \tag{3.9}$$

Where $\alpha_p$ is a number calculated representing proliferation by the stalk cells. For cells to proliferate they need space, so the algorithm measures the level of proliferation at each available sites (within a cell radii of the current position), averaging it in the end by the number of those sites (available sites are considered all points that pass all restrictions set by the algorithm). The flow of the algorithm is detailed in Figure 3.5.

## 3.7 Overall program

Using the mechanisms described above we can construct a program to simulate the angiogenesis process. Using the finite differences method for the update of the fields involved ($\phi$, $\omega$ and V (VEGF)), and the equations in Chapter 2.

The fluxogram below (Figure 3.6) shows a representation of the flow of the program used for the simulations of angiogenesis:

For the exploration of the model, several constants were made easily modifiable, including $\alpha$ the adhesion constant, $F$ the maximum amplitude of the force, $\mu_1$ the rigidity difference between the two phases (endothelial cells and extracellular matrix), the diffusion constant of $\phi$ and the diffusion, the consumption constants related to VEGF concentration and the constants related to the proliferation term ($P_{max}$ and $V_{max}$). The variation of some of these

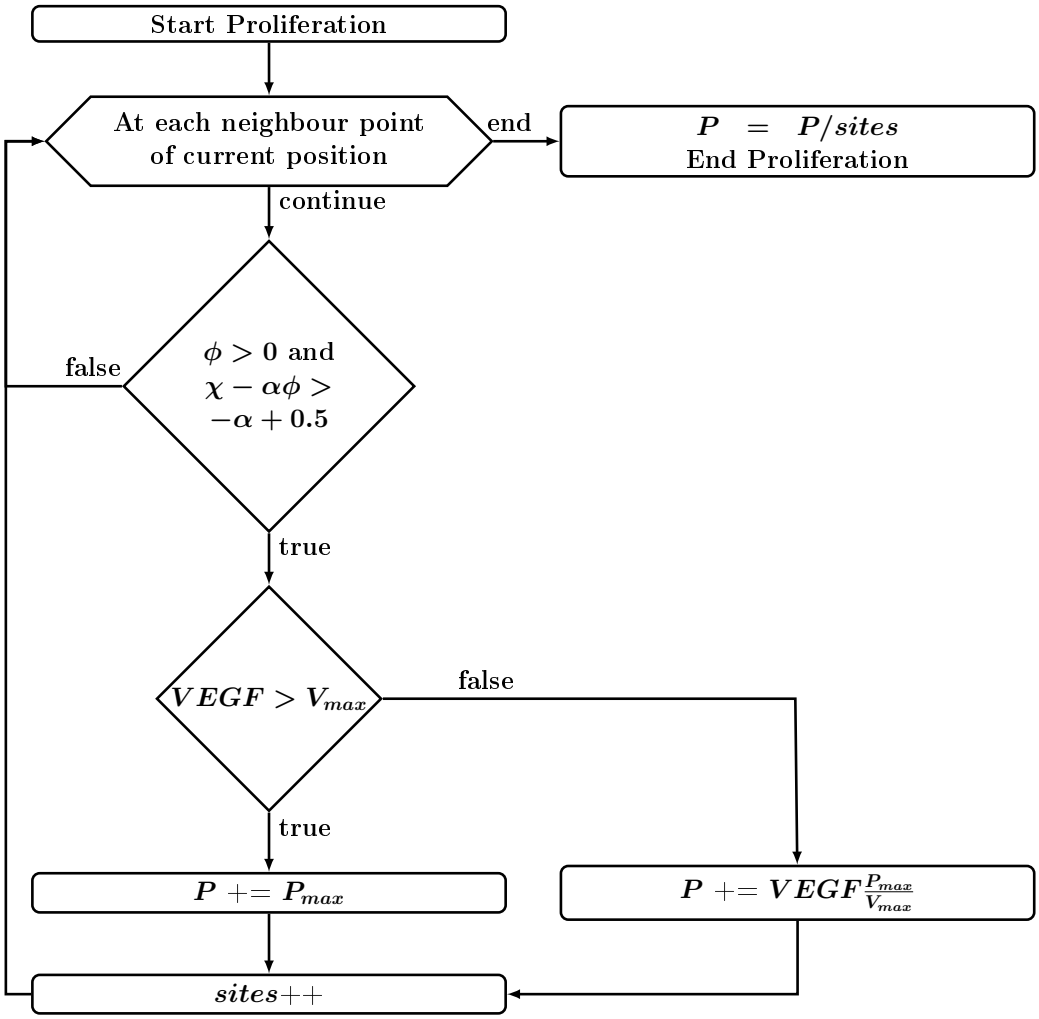


FIGURE 3.5: Fluxogram of the algorithm that determines the level of proliferation at each point of the lattice and each time step.

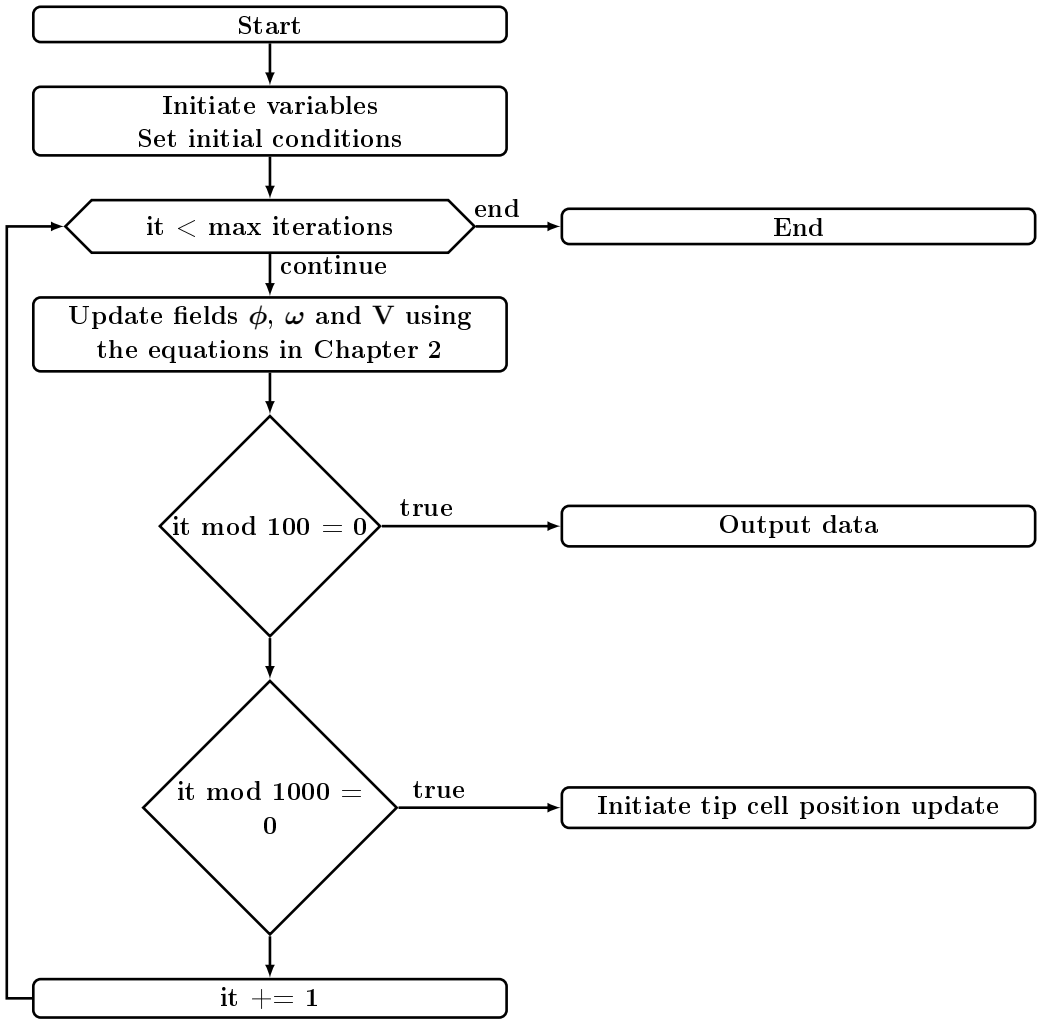


FIGURE 3.6: Flow of the overall program, starting with the setup of initial conditions, the iteration through time and, the regular output of data and update of the tip cell position.

constants allows to get a stable system, as well as the study of the system response under different conditions and situations.

# Chapter 4

# Model Exploration

As mentioned in Chapter 3, the overall coding effort was done to allow an easy exploration of the model, by changing the size of the system or the parameters that affect the system's responses. Having a stable system, the first study was done on changing the magnitude of the force that the tip cell can apply versus the adhesion constant of the system (vessel). In this study it was measured the distance that the tip cell covered in a certain amount of time for each pair of constants values, resulting in the following graph:

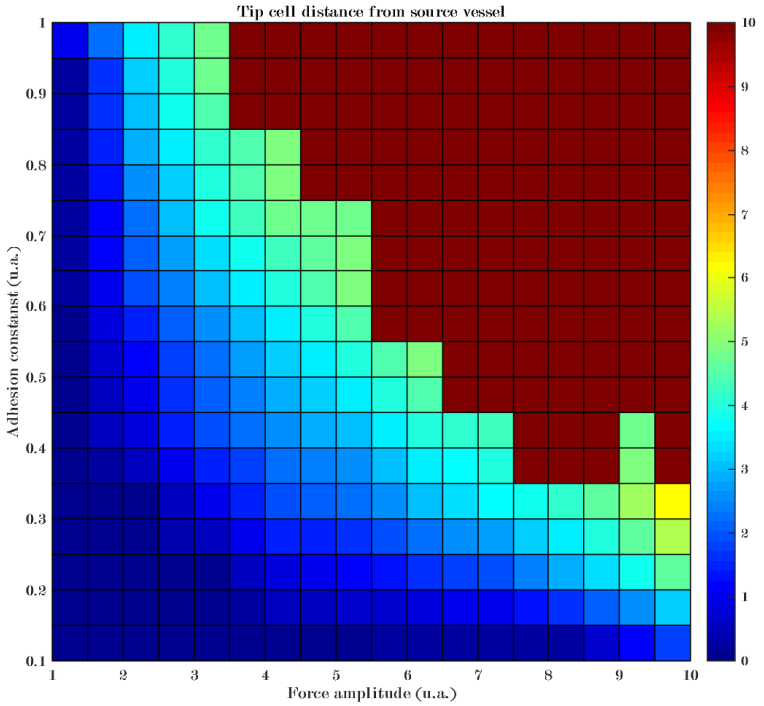


FIGURE 4.1: The distance that the tip cell can reach in a certain amount of time for varying values of adhesion and maximum force amplitude. We can see that generally higher forces and adhesion leads to greater distances travelled. The distance value of 10 was given to simulations where the tip cell disconnect from the main vessel.

Here we can see that generally higher values of both constants leads to bigger distances travelled by the vessel. The dark red area of the Figure 4.1 are the situations where the tip cell is disconnected from the source vessel.

As discussed in Chapter 1 the cell-ECM adhesion regulates the tip cell movement rate. So low adhesion constant leads to slower tip cell, but also allows more time for the rest of the vessel to adjust to the changes from that movement. In this regime the vessel maintains connection at all values of tip cell force simulated, as see in Figure 4.1. As the adhesion constant rises so does the tip cell movement and the less time the order parameter has to

compensate. This leads to tip cell disconnections at lower values of force and high adhesion constant.

The force applied is an important property of the tip cell phenotype. Here we see that higher forces lead to longer sprouts up to a point, beyond which the force leads the tip cell to break away from the main vessel. In the overall graph we see a competition between these two parameters, as high forces need small adhesion constants to remain connected while the opposite is also true. We can see it as low adhesion slows down the cell due to low focal adhesion sites which limits the movement regardless of the force the tip cell is trying to apply effectively giving time for the surrounding tissue to adjust to the tip cell movement. In high adhesion conditions the force must be small so that even if there many FAs because the force is low the tip cell moves slower that it theoretically could in those adhesion conditions.

An example simulation used for the graph above is shown in Figure 4.2.

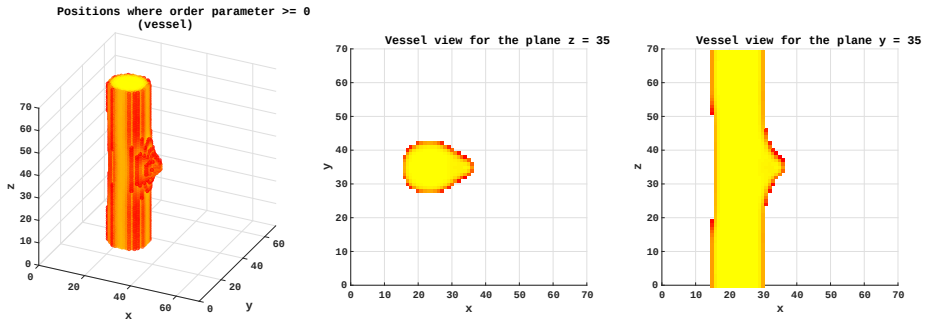


FIGURE 4.2: One example of the simulations used for the construction of the phase diagram of Figure 4.1. Here shown three separate views one where we have the three dimensional view, the middle image is a top view and the right most a side view of the system. (the x direction is the tip cell movement)

The following graph (Figure 4.3) shows the position over time of the tip cell for some of the simulations used to construct the phase diagram discussed above.

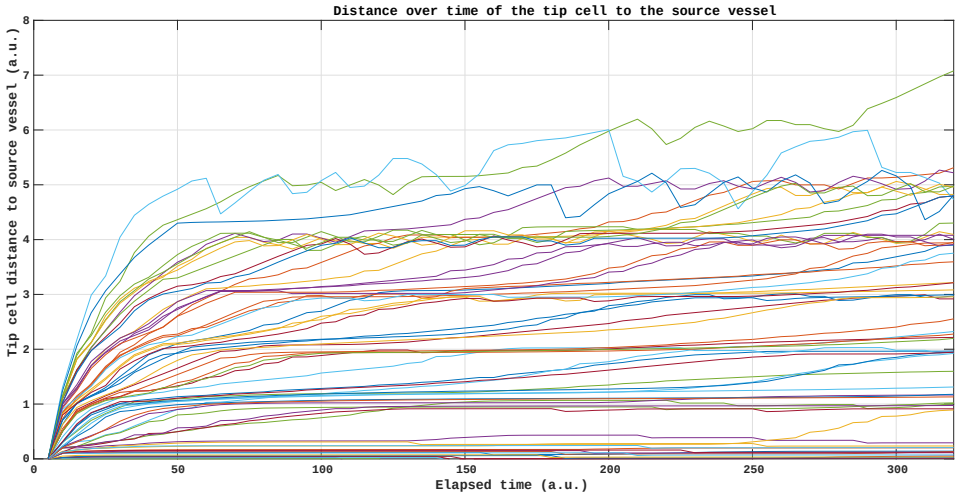


FIGURE 4.3: Here is shown the position over time of the tip cell for all simulations used for the Figure 4.1 that do not result in tip cell disconnection.

Here we can see some interesting behaviours some of which will be detailed below. In general though the tip cell moves rapidly in the beginning of the simulation quickly slowing down to the point where its position is almost static. Others break this observation continuing to move through out the simulation slowing down, but not enough that their position does not change visibly.

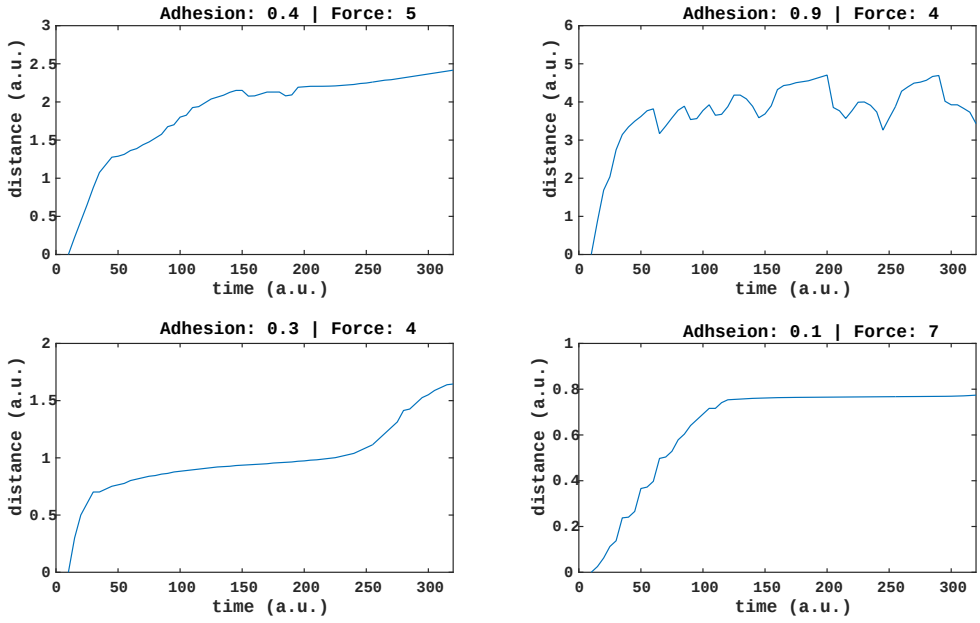


FIGURE 4.4: Four cases that show a few different behaviours of the tip cell movement under different values.

The example in the top left of Figure 4.4 shows a case where the position of the tip cell moves continuously more or less in the same direction through out the time simulated, this case represents a case of a balance of adhesion and the tip cell forces, but eventually, as with the other simulations in this group, the movement will slow down. The balance leads to a more gradual growth and not necessarily to a longer sprout. On the other hand the top right graph illustrates the case were there is a small force applied but a big adhesion constant leading to a pattern where the tip cell tries to move forward but, because of the adhesion, it is pulled back towards the source vessel as seen by the distance of the tip cell growing to, after a time, shrink back as seen in the figure. When there is a relatively small force and adhesion constants (bottom left of the figure) there is an initial burst followed by an almost stabilisation of the distance only to get a new burst as seen in the plotted data. Finally the last (bottom right) shows a case where the position stabilizes and practically does not grow from that point on.

In Figure 4.5 we show a case where the tip cell breaks away. In this models such a small dominion cannot be stable and rapidly disappears (see the $\phi$ values for the area of the tip cell). Because of this when the tip cell tries to update its position, there is no suitable position, becoming stuck in the same point for the rest of the simulation as seen on the position over time.

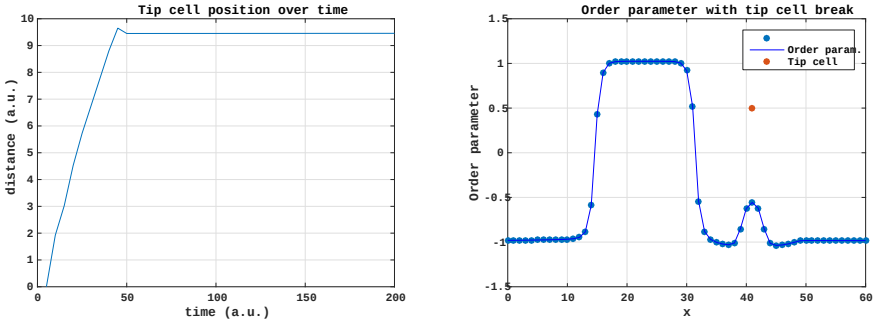


FIGURE 4.5: In this simulation the conditions set leads the tip cell to break away from the main vessel. The graph on the left shows the tip cell position over time while the right shows a slice of the order parameter ($z = y = 35$) that passes through the position of the tip cell. It is noteworthy that the area of the tip cell, while has $\phi > -1$, does not count as a vessel as defined in this work.

## 4.1 Anastomosis

Anastomosis happens when either two tip cells meet or when a tip cell encounters some other vessel. This forms a loop in the new vessel structure permitting then its eventual maturation and support for blood flow and irrigation of the hypoxia area. The following results shows the simulation of this mechanism in the used model (see Figure 4.6).

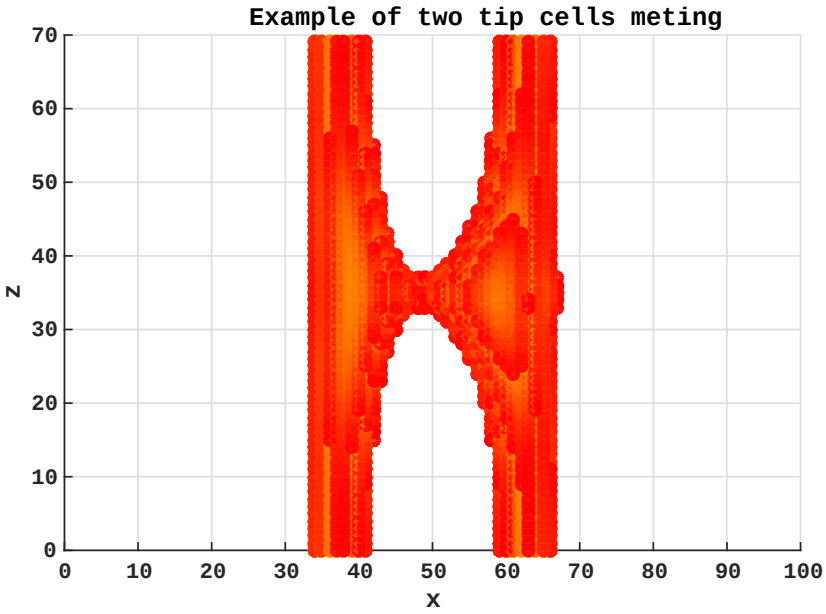


FIGURE 4.6: A simulation where two tip cells start form two parallel vessels and eventually meet in the center, where there is a source of VEGF.

As with the results in the previous section, the tip cells are quite limited in the distance they can cover, leading to, in this simulation, the close proximity of source vessels. Still the ability for this model to simulate this type of events is a good indicator of the model's capabilities.

In Figure 4.7 is shown the field $\omega$ in two distinct moments in time in this simulation. The one on the left being the displacements field in the beginning noting clearly defined red regions, while in the graph on the right (taken at the time of anastomosis) shows the two regions blending together. This connection permits maintaining the newly formed link even

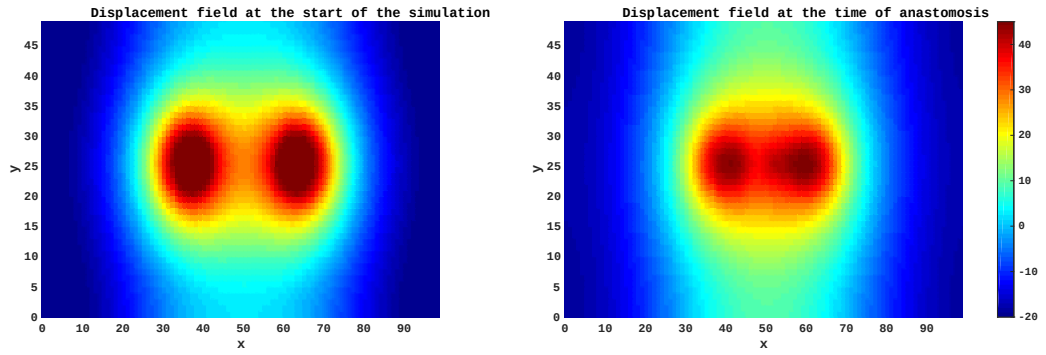


FIGURE 4.7: On the left the starting displacement field for the plane $z = 35$ and, on the right, we see the same but for the moment where the anastomosis happens.

as the tip cells disappear (when the two vessels meet, the blood is able to irrigate the tissue, the cells in hypoxia stop producing VEGF, and therefore the source of VEGF is not considered after that time).

## 4.2 Proliferation

In this section it will be discussed the results when cell proliferation was added to study its effects on the system and its responses.

In the Figure 4.8 is plotted the distance over time of the tip cell for the case where proliferation is present. This show us a continuous movement where instead of slowing down the vessel maintains its speed and, with the proliferation providing cell material for this growth, to continue indefinitely.

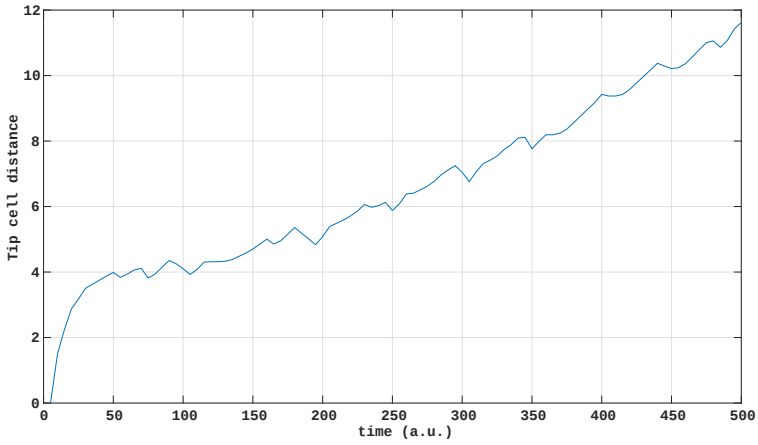


FIGURE 4.8: Time evolution of the position of the tip cell in the conditions where proliferation is present

Its noticeable how the tip cell movement is improved due to the proliferation from the stalk cells in the areas where proliferation is active (just behind the tip cell). The vessel becomes thicker and longer than in the situation where no proliferation was present (see Figure 4.9a).

In the base model, when a tip cell breaks from the main vessel, it is not stable (the corresponding $\phi$ domain disappears). However with the inclusion of proliferation it is possible for that domain to be stable and continue to move towards the source of VEGF. In Figure 4.9b is shown one example of this behaviour, that requires the applied force and adhesion

constant to be high enough for the tip cell to break away leaving proliferation to maintain the breakaway domain.

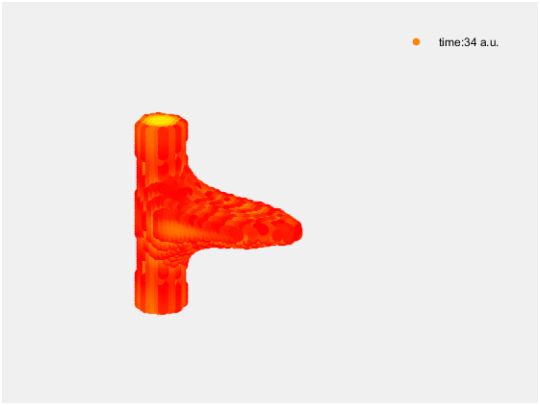


(A) View of a simulation with proliferation. We can see that the new vessel grows extensively. This simulation is also the source of the figure above.

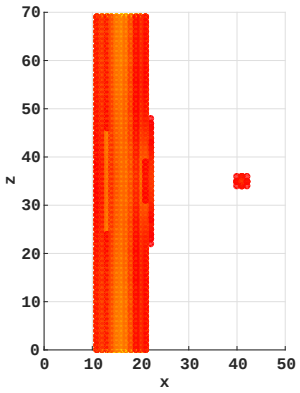


(B) A simulation where the tip cell breaks from the main vessel and a part of the dominion follows, sustained by the proliferation as this would not be possible without it.

FIGURE 4.9

As with the case for the system without proliferation, when including it the graph of force versus adhesion can be redone allowing a visual comparison between the two instances of the model. This data is represented in the figure below (Figure 4.10).

In the graph above we can see many differences between it and the one without proliferation. As expected, the inclusion of proliferation made higher values, of both adhesion and force, able to sustain the connection of the tip cell to the main vessel. Furthermore in these results we find that a balance of the values of both variables leads to a higher distance without the tip cell breaking.

In our model the proliferation is tied to the applied forces in this system, meaning that the proliferation occurs near the tip cell and is dependent on the force that it applies in the system. Higher tip cell force leads to more locations being available for proliferation. The opposite is true for low force amplitude. The adhesion constant works in a similar way. When this value is high, the threshold for a point to be considered for proliferation is lowered (specially for points near the order parameter's interface) leading to more proliferation and bigger distance covered by the tip cell in those conditions.

In the Figure 4.11 we calculated the terminal velocity of the tip cell in each displayed case. We can note that where the tip cell breaks from the main vessel, it slows down, likely due to have less proliferation helping in its movement. From the rest of the results it shows that the higher the values of force and adhesion the faster the tip cell moves through the system.

In Figure 4.12 we also see differences between the case with and without proliferation. While in the case without proliferation the tip cell movement would eventually slow down, here such a behaviour is not observed in many cases. Indeed most simulations done here point to a sustained movement where the proliferation can guarantee the connection between the growing sprout and the source vessel. However this was done with one value for the maximum proliferation. Using other values would likely yield different results some akin to these we present in the figure and other where, despite the presence of proliferation the tip cell would slow down or separate from the vessel as shown in the case where proliferation was not present.

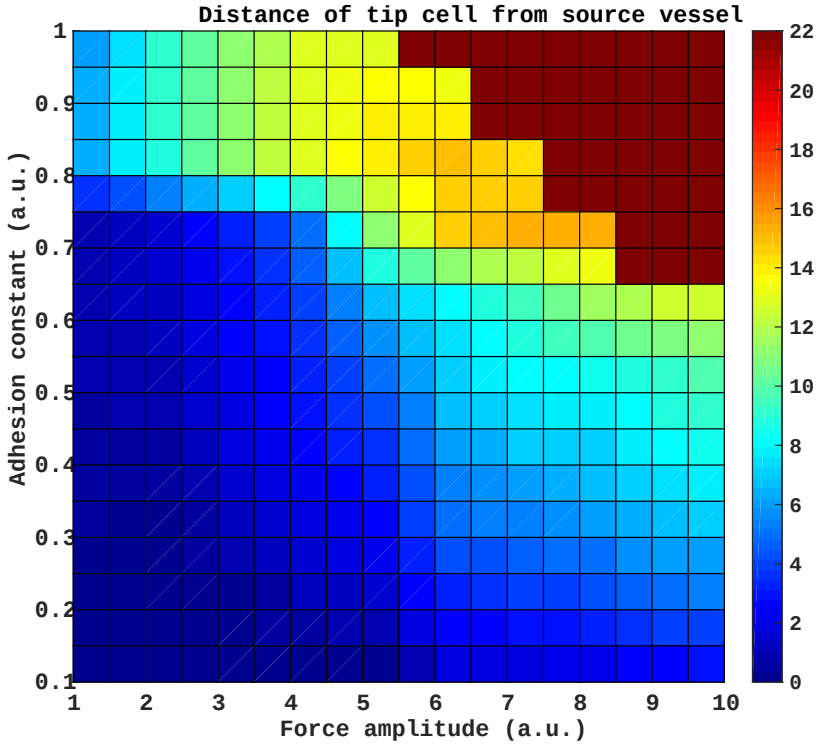


FIGURE 4.10: Here is shown the distance of the tip cell after some time for the system including proliferation for varying values of adhesion and applied force. The differences are very noticeable from the Figure 4.1. The data with value 22 where simulations where the tip cell would break away from the main vessel.

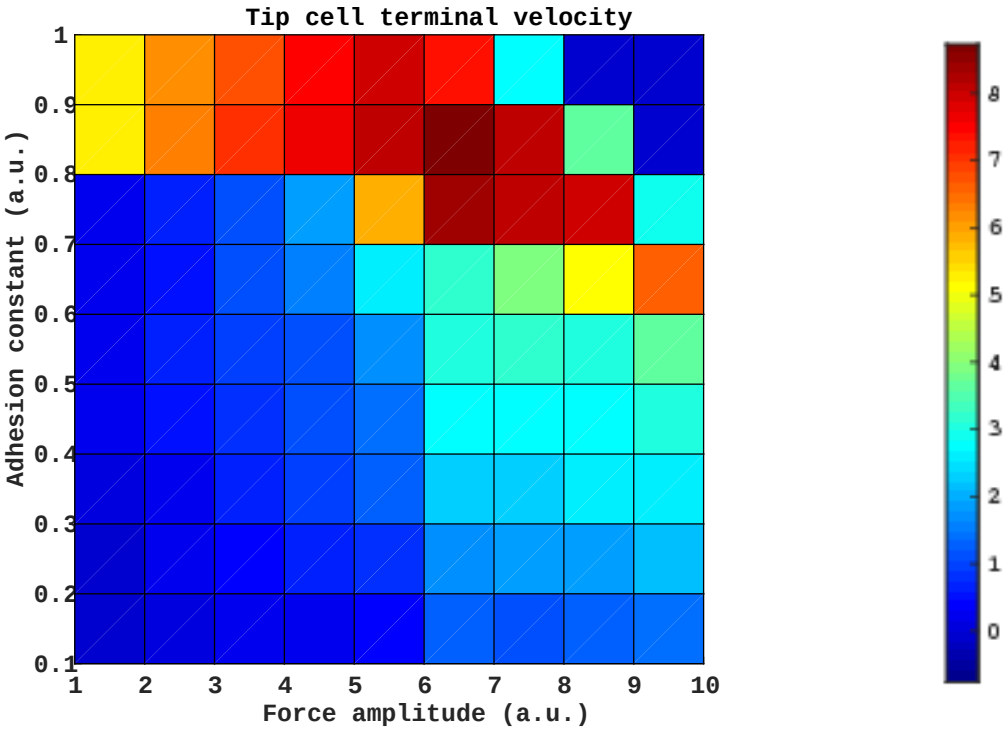


FIGURE 4.11: This graph includes the terminal velocity of the tip cell in each case studied for this purpose.

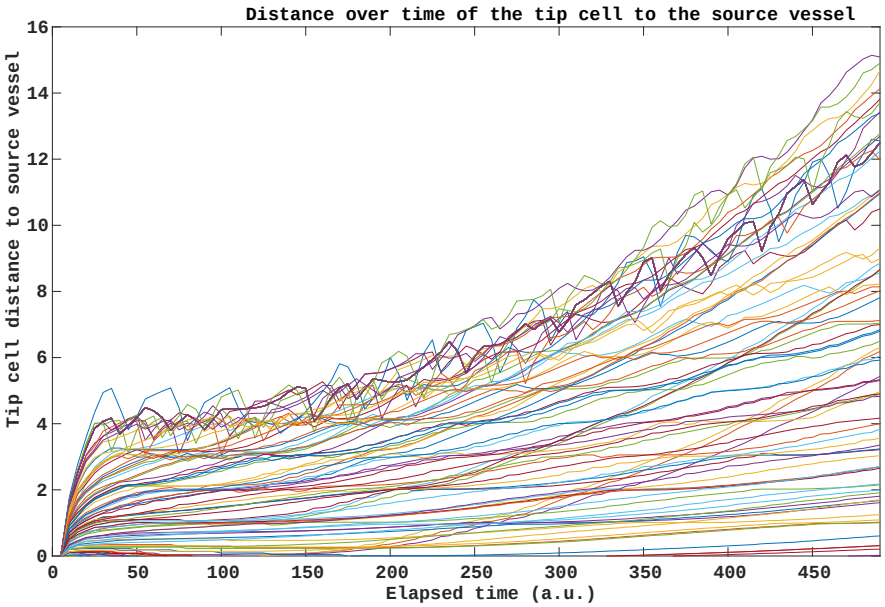


FIGURE 4.12: The position over time of the simulations, that did not result in the tip cell breaking away, that where used to build the graph in Figure 4.10

# Chapter 5

# Conclusion

In this work we derived a model for angiogenesis that includes the mechanical properties of the system in a three dimensional environment. Indeed, we observed the expected behaviour of the models, forming a sprout starting in the main vessel and growing form there, with the tip cell at the forefront of the growing vessel.

Initially it was studied the system response to varying values of the force the tip cells applied as they try to move and varying the adhesion constant of the model. This study is condensed in Figure 4.1. From this information we gather that there must be a balance to the values chosen for those two parameters, as if chosen to be too big leads to the tip cell breaking away from the main vessel. High adhesion means a strong connection between cells and ECM, giving more support to the cell, leading to a more effective movement, even with low forces. Low adhesion slows the cell by virtue of the small amount of connections meaning the cell is supported as well and, as it tries to apply force, very little happens as the cell have few points to gain traction as use the force effectively.

The next step was the study of the interaction between two tip cells following the same source of VEGF. To that end a simulation was done with two initial vessels each with a tip cell, and a source of VEGF in between the two vessels. Although the set of variables was quite strict in order for anastomosis to occur it was found a simulation in which the tip cells did manage to connect the two source vessels together. It would be interesting to try the simulation of anastomosis with the presence of cell proliferation.

The introduction of proliferation in the system changed noticeably its responses. The study of those responses came next. In one of the first simulations done we found a behaviour that could not happen before: sustained growth of the new vessel, where the tip cell moved in a consistent speed laying the foundations for the new sprout to grow behind it. Another situation, that could not happen in the case without proliferation, was when a tip cell would break away but now, thanks to proliferation in the system, the breakaway $\phi$ dominion could survive and move unimpeded.

To further compare the model with proliferation and without, we did another graph varying the force and the adhesion strength and collecting the new results in a similar fashion to the case without proliferation. We find, as expected, a few differences between the two sets of simulations. The first and most obvious was that, thanks to the proliferation, situations where, before, the tip cell would break could now sustain themselves and maintain a connection. Furthermore we found the results could be tied to our model for the proliferation and the conditions for it to occur such as the need to be near the interface of $\phi$ and to be near the tip cell (under the influence of the force).

It was also found that, with this particular set of chosen parameters for the proliferation, all simulations presented a behaviour of sustained tip cell movement, meaning that the tip cell could continue to move indefinitely. However it would yield different results with other values for the maximum proliferation, and a further study of the proliferation model could yield more information of the responses of the system under different conditions.

This work, as every other in science, is grounded on work that came before. In the paper "Force at the tip: Modelling tension and proliferation in sprouting angiogenesis" [30], this model was studied in a two dimensional environment. It is good then to make a comparison between the results obtained in that paper and the ones presented in this work.

One of the more noticeable differences come from visual cues, while in 2D the main vessel seems to curve and bend easily as the tip cell applies forces, the same is not seen in the 3D results. Instead the main vessel remains strait under the forces of the tip cell. Another difference possibly related is that the movement of the tip cell seems much more constrained, seemingly experiencing more resistance to its movement in the three dimensional environment as opposed to the 2D one.

A possible cause for these differences of the model responses in different dimensional environments may stem from connectivity. This concept comes from image processing, and relates the way a point in a lattice space (in image processing this would be a single pixel) is connected to its neighbours. In a 2D lattice, and considering the first neighbours only, the space is 4-connected, meaning that each point has 4 neighbours. Following the same logic for 3D, this space is 6-connected. This would mean that each point is affected from more sources in 3D than in 2D, especially considering that the model involves up to fourth order derivatives, leading to, for a variation in the system to "survive" it needs to have higher magnitude lest it be diffused by its neighbours.

# Chapter 6

# Future Work

In this work the three dimensional model was implemented and tested. There are, however more that can be done with models possibly yielding new and better information of the mechanisms here modelled.

One possible avenue of improving the models lies in a more in depth analysis of the proliferation term and its associated constants to better understand the impact that this mechanism has on the overall model of angiogenesis. This would also benefit from further study to match the constants of this term to situation found on laboratory experiments as a way to both improve the model and serve as validation for it. The shape of the vessel could also be studied as a function of the spacial dependence of the force exerted by the tip cell.

In this work the extracellular matrix was considered homogeneous and isotropic but, in reality, this is rarely the case thus a model of the ECM with variations of the local rigidity would be an interesting next step for the model and for the study of how these variations could change the system response and interfere with tip cell movement.

Related to the previous point, the model could be adapted to study the tip cell movement (and new vessel growth) near an interface between ECMs with different rigidities. This could provide useful information since different tissues can have different ECM rigidities and angiogenesis should be able to deal with those situations.

Finally as with all computational models, one important step is its use for a real word case and, using all the tools that the model provides, try to better understand that case and maybe devise a possible way to change it.

# Appendix A

# Derivative free energy functional

The free energy equation is:

$$F[\phi(\mathbf{r},t)] = \int \rho_\phi \left( -\frac{a\phi^2}{2} + \frac{\phi^4}{4} + \frac{\epsilon^2}{2}(\nabla\phi)^2 \right) d\mathbf{r} \tag{A.1}$$

Introducing a small function $\delta\phi$ we get (considering only terms to first order):

$$\begin{aligned} F[\phi+\delta\phi] = \int \rho_\phi \left( -\frac{a(\phi+\delta\phi)^2}{2} + \frac{(\phi+\delta\phi)^4}{4} + \frac{\epsilon^2}{2}(\nabla(\phi+\delta\phi))^2 \right) d\mathbf{r} = \\ \int \rho_\phi \left( -\frac{a\phi^2}{2} - a\phi\delta\phi + \frac{\phi^4}{4} + \phi^3\delta\phi + \frac{\epsilon^2}{2}(\nabla\phi+\nabla\delta\phi))^2 \right) d\mathbf{r} = \\ F[\phi] + \int \rho_\phi \left( -a\phi\delta\phi + \phi^3\delta\phi + \epsilon^2\nabla\phi\nabla\delta\phi \right) d\mathbf{r} = \end{aligned} \tag{A.2}$$

Using the derivative definition:

$$\delta F = \int \frac{\delta F}{\delta\phi}\delta\phi d\mathbf{r} \tag{A.3}$$

$$\delta F = \int \rho_\phi \left( -a\phi\delta\phi + \phi^3\delta\phi - \epsilon^2\delta\phi\nabla^2\phi \right) d\mathbf{r} \Leftrightarrow \tag{A.4}$$

$$\frac{\delta F}{\delta\phi} = \rho_\phi \left( -a\phi + \phi^3 - \epsilon^2\nabla^2\phi \right) \tag{A.5}$$

# Appendix B

# Derivation of $\omega$ field equation

The elastic free energy contribution has the form:

$$F_{ele}[\phi, \mathbf{u}(\mathbf{r})] = \int d\mathbf{r} \frac{1}{2} \sigma_{ij} \varepsilon_{ij} \tag{B.1}$$

Using the definitions of $\sigma$ and $\varepsilon$ yields:

$$F_{ele}[\phi, \mathbf{u}(\mathbf{r})] = \int \left[ \frac{1}{4} \left( K - \frac{2\mu}{d} \right) \varepsilon_{kk} \varepsilon_{jj} + \frac{\mu}{2} \varepsilon_{ij} \varepsilon_{ij} \right] d\mathbf{r} =$$

$$= \int \left[ \frac{1}{2} \left( K - \frac{2\mu}{d} \right) \partial_k u_k \partial_j u_j + \frac{\mu}{2} (\partial_i u_j + \partial_j u_i)(\partial_i u_j + \partial_j u_i) \right] d\mathbf{r} =$$

$$= \int \left[ \frac{1}{2} \left( K - \frac{2\mu}{d} \right) \partial_k u_k \partial_j u_j + \mu (\partial_i u_j \partial_i u_j + \partial_j u_i \partial_i u_j) \right] d\mathbf{r} \tag{B.2}$$

Introducing small variation $\delta u$:

$$F_{ele}[u + \delta u] = \int \left[ \frac{1}{2} \left( K - \frac{2\mu}{d} \right) \partial_k (u_k + \delta u_k) \partial_j (u_j + \delta u_j) + \right.$$

$$\left. + \mu \Big( \partial_i (u_j + \delta u_j) \partial_i (u_j + \delta u_j) + \partial_j (u_i + \delta u_i) \partial_i (u_j + \delta u_j) \Big) \right] d\mathbf{r} \tag{B.3}$$

Separating all terms and ignoring those higher order then $\delta u$:

$$F_{ele}[u + \delta u] = \int \left[ \frac{1}{2} \left( K - \frac{2\mu}{d} \right) (\partial_k u_k \partial_j u_j + 2 \partial_k \delta u_k \partial_j u_j) + \right.$$

$$\left. + \mu \Big( \partial_i u_j \partial_i u_j + 2 \partial_i \delta u_j \partial_i u_j + \partial_j u_i \partial_i u_j + 2 \partial_j u_i \partial_i \delta u_j \Big) \right] d\mathbf{r} =$$

$$F_{ele}[u + \delta u] = F_{ele}[u] + \int \left[ \left( K - \frac{2\mu}{d} \right) \partial_k \delta u_k \partial_j u_j + 2\mu (\partial_i \delta u_j \partial_i u_j + \partial_j u_i \partial_i \delta u_j) \right] d\mathbf{r} \tag{B.4}$$

$$\delta F_{ele} = \int \left[ \left( K - \frac{2\mu}{d} \right) \partial_i \delta u_j \delta_{ij} \partial_k u_k + 2\mu (\partial_i \delta u_j \partial_i u_j + \partial_j u_i \partial_i \delta u_j) \right] d\mathbf{r} =$$

$$= \int \left[ \underbrace{\left[ \left( K - \frac{2\mu}{d} \right) \delta_{ij} \partial_k u_k + 2\mu (\partial_i u_j + \partial_i \delta u_j) \right]}_{\sigma_{ij}} \partial_j \delta u_i = \sigma_{ij} \partial_j \delta u_i \right] d\mathbf{r} \tag{B.5}$$

Therefore:

$$\frac{\delta F_{ele}}{\delta u_i} = -\partial_j \sigma_{ij} \tag{B.6}$$

$$\frac{\delta F_{ele}}{\delta u_i} = -\left(K - \frac{2\mu}{d}\right)\delta_{ij}\partial_j\partial_k u_k - 2\mu\partial_j(\partial_i u_j + \partial_j u_i) \tag{B.7}$$

Using this result we can redo the calculation now using $\mu = \mu_0 + \phi\mu_1$ and the split of the displacement field and free energy functional and using the $\omega$ field:

$$\begin{aligned}\frac{\delta F_{ele}}{\delta u_i} &= -\left(K - \frac{2\mu}{d}\right)\delta_{ij}\partial_j\partial_{kk}\omega - 2\mu(\partial_{ji}\partial_j\omega + \partial_{jj}\partial_i\omega) = \\ &= -\left(K - \frac{2\mu}{d} + \mu\right)\partial_{ijj}\omega = -L_0\partial_{ijj}\omega\end{aligned} \tag{B.8}$$

Knowing that the functional derivative of $\frac{\delta F_f}{\delta u_i} = \partial_i\chi$ and that the system is in a mechanical equilibrium:

$$-L_0\partial_{ijj}\omega + \partial_i\chi = 0 \tag{B.9}$$

This has a solution:

$$L_0\partial_{jj}\omega = \chi \Leftrightarrow L_0\nabla^2\omega = \chi = -\alpha\phi + \chi^f \tag{B.10}$$

# Appendix C

# Derivation of mechanical energy terms

The total mechanical free energy is $F_{mec} = F_{ele} + F_f$. As before in Appendix B, using $\mu = \mu_0 + \phi\mu_1$ and the split of the displacement field and free energy functional and using the $\omega$ field, we obtain:

$$F_{ele} = \int \left[\frac{1}{2}\left(K - \frac{2\mu}{d}\right)\partial_k u_k \partial_j u_j - \mu(\partial_i u_j \partial_i u_j + \partial_i u_j \partial_j u_i)\right] d\mathbf{r} \tag{C.1}$$

$$F_{mec} = \int \left[\frac{1}{2}\left(K - \frac{2\mu}{d}\right)\partial_k u_k \partial_j u_j + \mu(\partial_i u_j \partial_i u_j + \partial_i u_j \partial_j u_i) - \chi\partial_i u_i\right] d\mathbf{r} \tag{C.2}$$

Collecting the zeroth order terms:

$$F^0_{mec} = \int \left[\frac{1}{2}\left(K - \frac{2\mu_0}{d}\right)\partial_{kk}\omega\partial_{jj}\omega + \mu_0(\partial_{ij}\omega\partial_{ij}\omega + \partial_{ij}\omega\partial_{ji}\omega) - \chi\partial_{ii}\omega\right] d\mathbf{r} =$$

$$= \int \left[\frac{1}{2}\left(K - \frac{2\mu_0}{d} + \mu_0\right)\partial_{kk}\omega\partial_{jj}\omega - \chi\partial_{ii}\omega\right] d\mathbf{r} \tag{C.3}$$

Using the equation found at Appendix B:

$$F^0_{mec} = \int \left[\frac{L_0}{2}\frac{\chi}{L_0}\frac{\chi}{L_0} - \chi\frac{\chi}{L_0}\right] d\mathbf{r} = -\int \frac{\chi^2}{2L_0} d\mathbf{r} \tag{C.4}$$

Now the same needs to be done for the first order terms. These ones will have some overlap between $u^0$ and $u^1$. The equation for $F^1_{mec}$ is:

$$F^1_{mec} = \int \left[\frac{1}{2}\left[\left(\frac{2\mu_1\phi}{d}\right)\partial_i u^0_i \partial_j u^0_j + \left(K - \frac{2\mu_0}{d}\right)\partial_i u^1_i \partial_j u^0_j + \left(K - \frac{2\mu_0}{d}\right)\partial_i u^0_i \partial_j u^1_j\right] -\right.$$

$$\left. - \frac{\mu_1\phi}{2}\left(\partial_i u^0_j \partial_i u^0_j + \partial_i u^0_j \partial_j u^0_i\right) + \frac{\mu_0}{2}\left(\partial_i u^1_j \partial_i u^0_j + \partial_i u^1_j \partial_j u^0_i + \partial_i u^0_j \partial_i u^1_j + \partial_i u^0_j \partial_j u^1_i\right) - \chi\partial_i u^1_i\right] d\mathbf{r} \tag{C.5}$$

Using the relation $u^0_i = \partial_i w$:

$$F^1_{mec} = \int \left[\frac{\mu_1\phi}{d}\nabla^2\omega\nabla^2\omega + \left(K - \frac{2\mu_0}{d}\right)\partial_i u^1_i \nabla^2\omega - \frac{\mu_1\phi}{2}\left(\partial_{ij}\omega\partial_{ij}\omega + \partial_{ij}\omega\partial_{ji}\omega\right) +\right.$$

$$\left. + \mu_0\left(\partial_i u^1_j \partial_{ij}\omega + \partial_i u^1_j \partial_{ji}\omega\right) - \chi\partial_i u^1_i\right] d\mathbf{r} \tag{C.6}$$

$$F^1_{mec} = -\int \left[ \mu_1 \phi \left( \partial_{ij}\omega \partial_{ij}\omega - \frac{1}{d}(\nabla^2\omega)^2 \right) + \partial_i u^1_i \left[ \left( K - \frac{2\mu_0}{d} \right) \partial_{jj}\omega - \chi \right] + 2\mu_0 \partial_i u^1_j \partial_{ij}\omega \right] d\mathbf{r} \tag{C.7}$$

$$F^1_{mec} = -\int \left[ \mu_1 \phi \left( \partial_{ij}\omega \partial_{ij}\omega - \frac{1}{d}(\nabla^2\omega)^2 \right) + u^1_i \underbrace{\left[ \left( K - \frac{2\mu_0}{d} \right) \partial_{ijj}\omega - \partial_i \chi + 2\mu_0 \partial_{ijj}\omega \right]}_{=0} \right] d\mathbf{r} \tag{C.8}$$

The equation for the first order contribution of mechanical term is:

$$F^1_{mec} = -\int \mu_1 \phi \left( \partial_{ij}\omega \partial_{ij}\omega - \frac{1}{d}(\nabla^2\omega)^2 \right) d\mathbf{r} \tag{C.9}$$

The total contribution yields:

$$F_{mec} = -\int \left[ \mu_1 \phi \left( \partial_{ij}\omega \partial_{ij}\omega - \frac{1}{d}(\nabla^2\omega)^2 \right) + \frac{\chi^2}{2L_0} \right] d\mathbf{r} \tag{C.10}$$

# Appendix D

# Derivation total free energy functional

The total free energy functional is:

$$F[\phi(\mathbf{r}),\mathbf{u}(\mathbf{r})]=\int\left[\rho_\phi\left(-\frac{a\phi^2}{2}+\frac{\phi^4}{4}+\frac{\epsilon^2}{2}(\nabla^2\phi)^2\right)-\frac{\chi^2}{2L_0}-\mu_1\phi\left(\partial_{ij}\omega\partial_{ij}\omega-\frac{1}{d}(\nabla^2\omega)^2\right)\right]d\mathbf{r} \tag{D.1}$$

Introducing a small variation $\delta\phi$. As the first part of this derivation was already shown in Appendix A here the focus will be given to the elastic part of the free energy:

$$F[\phi+\delta\phi]=-\int\left[\frac{(-\alpha(\phi+\delta\phi)+\chi^f)^2}{2L_0}-\mu_1(\phi+\delta\phi)\left(\partial_{ij}(\omega+\delta\omega)\partial_{ij}(\omega+\delta\omega)-\right.\right.$$
$$\left.\left.-\frac{1}{d}(\nabla^2(\omega+\delta\omega))^2\right)\right]d\mathbf{r} \tag{D.2}$$

Keeping only variations of first order:

$$F[\phi+\delta\phi]=-\int\left[\frac{\chi^2}{2L_0}+\frac{\alpha\chi\delta\phi}{L_0}-\mu_1\phi\left(\partial_{ij}\omega\partial_{ij}\omega+2\partial_{ij}\omega\partial_{ij}\delta\omega-\frac{1}{d}((\nabla^2\omega)^2+2\nabla^2\omega\nabla^2\delta\omega)\right)-\right.$$
$$\left.-\mu_1\delta\phi\left(\partial_{ij}\omega\partial_{ij}\omega+2\partial_{ij}\omega\partial_{ij}\delta\omega-\frac{1}{d}((\nabla^2\omega)^2+2\nabla^2\omega\nabla^2\delta\omega)\right)\right]d\mathbf{r} \tag{D.3}$$

Using the equation for $\omega$ we get the relation:

$$\nabla^2\delta\omega=\partial_{jj}\delta\omega=-\frac{\alpha}{L_0}\delta\phi \tag{D.4}$$

The equation above becomes:

$$F[\phi+\delta\phi]=-\int\left[\frac{\chi^2}{2L_0}+\frac{\alpha\chi\delta\phi}{L_0}-\mu_1\delta\phi\left(\partial_{ij}\omega\partial_{ij}\omega-\frac{1}{d}(\nabla^2\omega)^2\right)-\right.$$
$$\left.-\mu_1\phi\left(\partial_{ij}\omega\partial_{ij}\omega+2\partial_{ij}\omega\partial_{ij}\delta\omega-\frac{1}{d}\big((\nabla^2\omega)^2-\frac{2\alpha}{L_0}\delta\phi\nabla^2\omega\big)\right)\right]d\mathbf{r} \tag{D.5}$$

$$\delta F=\int\left[\frac{\alpha\chi\delta\phi}{L_0}+\frac{2\mu_1\alpha}{L_0}\phi\left(\partial_{ij}\omega\partial_{ij}\frac{1}{\partial_{ii}}\delta\phi-\frac{\delta\phi}{d}\nabla^2\omega)\right)-\mu_1\delta\phi\left(\partial_{ij}\omega\partial_{ij}\omega-\frac{1}{d}(\nabla^2\omega)^2\right)\right]d\mathbf{r} \tag{D.6}$$

Leading to the final equation:

$$\frac{\delta F}{\delta \phi} = \rho_\phi(-a\phi + \phi^3 - \epsilon^2\nabla^2\phi) + \frac{\alpha\chi}{L_0} + \frac{2\mu_1\alpha}{L_0}\left(\frac{1}{\nabla^2}\partial_{ij}(\phi\partial_{ij}\omega) - \frac{1}{d}\phi\nabla^2\omega)\right) - \\ - \mu_1\left(\partial_{ij}\omega\partial_{ij}\omega - \frac{1}{d}(\nabla^2\omega)^2\right) \quad \text{(D.7)}$$

Unfolding $\chi$ and setting $a$ such that $a - \frac{\alpha^2}{L_0\rho_\phi} = 1$ yields the final equation displayed in Chapter 2:

$$\frac{\delta F}{\delta \phi} = \rho_\phi(-\phi + \phi^3 - \epsilon^2\nabla^2\phi) + \frac{\alpha\chi^f}{L_0} - \mu_1\left(\partial_{ij}\omega\partial_{ij}\omega - \frac{1}{d}(\nabla^2\omega)^2\right) + \\ + \frac{2\mu_1\alpha}{L_0}\left(\frac{1}{\nabla^2}\partial_{ij}(\phi\,\partial_{ij}\omega) - \frac{\phi}{d}\nabla^2\omega)\right) \quad \text{(D.8)}$$

# Bibliography


[1] D. Ribatti and E. Crivellato, “"sprouting angiogenesis", a reappraisal”, *Developmental Biology*, vol. 372, pp. 38–47, 2012.

[2] B. M. Prior and H. T. Yang, “What makes vessels grow with exercise training?”, *Journal of Applied Physiology*, vol. 97, pp. 157–165, 2004.

[3] A. Minchenko, T. Bauer, S. Salceda, and J. Caro, “Hypoxic stimulation of vascular endothelial growth factor expression in vitro and in vivo”, *Journal of Technical Methods and Pathology*, vol. 73, pp. 374–379, 1994.

[4] A. L. Harris, “Hypoxia - a key regulatory factor in tumour growth”, *Nature*, vol. 2, pp. 38–47, 2002.

[5] (2016). Biosym, [Online]. Available: `http://web.mit.edu/smart/research/biosym/BioSyM-Research-Thrust%203-Archives.html`.

[6] H. M. Eilken and R. H. Adams, “Dynamics of endothelial cell behaviour in sprouting angiogenesis”, *Curent Opinion in Cell Biology*, vol. 22, pp. 617–625, 2010.

[7] F. D. Smet, I. Segura, P. Hohensinner, and P. Carmeliet, “Mechanisms of vessel branching: Filopodia on endothelial tip cells lead the way”, *Arteriosclerosis Thrombosis and Vascular Biology*, vol. 29, pp. 639–649, 2009.

[8] H. Gerhardt and C. Betsholtz, “How do endothelial cells orientate?”, *Mechanisms of Angiogenesis*, pp. 3–15, 2005.

[9] L. Lamalice, F. L. Boeuf, and J. Huot, “Endothelial cells migration during angiogenesis”, *Circulation Research*, vol. 100, pp. 782–794, 2007.

[10] M. Hellström, L.-K. Phng, and et al, “Dll4 signalling through notch1 regulates formation of tip cells during angiogenesis”, *Nature*, vol. 445, pp. 776–780, 2007.

[11] L. Jakobsson, C. A. Franco, and et al, “Endothelial cells dynamically compete for the tip cell position during angiogenic sprouting”, *Nature cell biology*, vol. 12, pp. 943–953, 2010.

[12] S. Goel, D. G. Duda, L. Xu, and L. L. Munn, “Normalization of the vasculature for treatment of cancer and other diseases”, *Physiological Reviews*, vol. 91, pp. 1071–1121, 2011.

[13] B. M. Gumbiner, “Cell adhesion: Review the molecular basis of tissue architecture and morphogenesis”, *Cell*, vol. 84, pp. 345–357, 1996.

[14] (2016). Cell adhesion, [Online]. Available: `https://www.mechanobio.info/topics/mechanosignaling/components-of-cell-adhesion/`.

[15] E. Dejana, M. Corada, and M. Lampugnani, “Endothelial cell-to-cell junctions”, *The FASEB Journal*, vol. 10, pp. 910–918, 1995.

[16] G. Bazzoni and E. Dejana, “Endothelial cell-to-cell junctions: Molecular orgaization and role in vascular homeostasis”, *Physiology Review*, vol. 84, pp. 869–901, 2004.

[17] P. Carmeliet, M.-G. Lampugnani, L. Moons, F. Breviario, and et al, “Targeted deficiency or cytosolic truncation of the ve-cadherin gene in mice impairs vegf-mediated endothelial survival and angiogenesis”, *Cell*, vol. 98, pp. 147–157, 1999.

[18] P. Navarro, L. Rucco, and E. Dejana, "Differential localization of ve- and n-cadherins in human endothelial cells: Ve-cadherin competes with n-cadherin for junctional localization", *The Journal of Cell Biology*, vol. 140, pp. 1475–1484, 1998.

[19] A. Shay-Salit, M. Shushy, E. Wolfovitz, H. Yahav, and et al., "Vegf receptor 2 and the adherens junction as a mechanical transducer in vascular endothelial cells", *Procedings of the National Academy of Sciences of the United States of America (PNAS)*, vol. 99, pp. 9462–9467, 2002.

[20] R. O. Hynes, "The extracellular matrix: Not just pretty fibrils", *Science*, vol. 326, pp. 1216–1219, 2009.

[21] J. E. Meredith, B. F. Jr., and M. A. Schwartz, "The extracellular matrix as a cell survival factor", *Molecular Biology of the Cell*, vol. 4, pp. 953–961, 1993.

[22] H. Hutchings, N. Ortega, and J. Plouet, "Extracellular matrix-bound vascular endothelial growth factor promotes endothelial cell adhesion, migration, and survival through integrin ligation", *The FASEB Journal*, vol. 17, pp. 1520–1522, 2001.

[23] S. K. Mitra, D. A. Hanson, and D. D. Schlaepfer, "Focal adhesion kinase: In command and control of cell motility", *Nature cell biology*, vol. 6, pp. 56–68, 2005.

[24] G. W. Brodland, "How computational models can help unlock biological systems", *Seminars in Cell & Developmental Biology*, vol. 48, pp. 62–73, 2015.

[25] J. Walpole, J. Papin, and S. Pierce, "Multiscale computational models of complex biological systems", *Annual Review of Biomedical Engineering*, vol. 15, pp. 137–154, 2013.

[26] A. L. Bauer, T. L. Jackson, and Y. Jiang, "A cell-based model exibiting branching and anastomosis during tumor-induced angiogenesis", *Biophysical Journal*, vol. 92, pp. 3105–3121, 2007.

[27] R. D. Travasso, E. C. Poiré, and et al, "Tumor angiogenesis and vascular paterning: A mathematical model", *PLoS one*, 2011.

[28] P. Carmeliet and R. K. Jain, "Angiogenesis in cancer and other diseases", *Nature*, vol. 407, pp. 249–257, 2000.

[29] C. Reinhart-King, M. Dembo, and D. Hammer, "The dynamics and mechanics of endothelial cell spreading", *Biophysical Journal*, vol. 89, pp. 676–689, 2005.

[30] P. Oliveira, R. Travasso, and D. D. Schlaepfer, "Force at the tip: Modelling tension and proliferation in sprouting angiogenesis", *PLOS computational biology*, 2015.